Scuola Internazionale Superiore di Studi Avanzati

Trieste, Italy

Neuronal Activity in Rat Hippocampus and Secondary Somatosensory Cortex during a Tactile Working Memory Task

Thesis submitted for the degree of

"*Doctor Philosophiæ*"

Candidate

Shima Talehy Moineddin

Advisor

Prof. Mathew E. Diamond

March 2016

Cognitive Neuroscience Sector

Acknowledgements

Almost ten years ago, when I participated in an influential workshop of neuroscience by IPM in Iran, I found what inspired me in science and decided to follow this field, then I got the dream of doing phd in neuroscince. It seems that I am on the way to my dream and there are many individuals who provided me support, both in the sense of academia and friendship in this path and I would like to show my gratitude towards them.

My special thanks go to my advisor, Mathew Diamond to whom I am truly indebted as he gave me support and freedom during my studies in his lab. From the first time we talked about my interests in neuroscience, he listened to me patiently and gave me the best advice from his experience and insight, the fortune that any student seeks.

I am also grateful to Rodrigo Quiroga, as my co-adviser who always supported me unconditionally and gave me the feeling that he had faith in me. Each time he visited us in SISSA, he carried loads of positive energy and I am sure I couldn't go through the progress reports' stress without him.

John Nicholls, from the first day of my phd until the writing up of the thesis, with his priceless comments kept teaching me how to be a good scientist and I am really grateful for this opportunity that he gave me.

I would like to thank Rafaella Rumiati as she made a favor to me at a critical point and I will never forget her help. I am thankful to Davide Zoccolan, as he followed my work the first two years of my phd.

I am grateful to Kambiz Pourrezaei, for the scientific approach he taught me and provided me with precious discussions.

I was so lucky to have my dear friend, Georgette Argiris who patiently helped me with correcting the writing style. It was so precious to me all the efforts she made despite being busy with her own work.

In the lab, I always found immediate help and support from the mechatronic team, Marco Gigante, Fabrizio Manzino, Fabio Meneghini, Erik Zorzin and Rudi Laco, all of them with their expertise provided outstanding technical help that made the time consuming and difficult work in the lab possible and I would like to thank them all. I am thankful to Francesa

Pulecchi, for help during surgeries, training and performing histology. Alfonso Malpede arrived in SISSA at the right time to help me with the trainings and without his help I couldn't focus on writing the thesis.

The comments and trainings I got from Romain Brassellet, Arash Fassihi and Vahid Esmaili helped me a lot on this path and I am thankful to them. I enjoyed working with Sergey Antopolskiy during acute surgery recordings and I would like to thank him.

I need to thank all those who provided me positive energy and encouraged me to go on despite difficulties; I want to thank Shima Seyed Allaei who welcomed me both in SISSA and Trieste and changed my life forever. Ladan Amin and Houman Safaai, were just like a family beside me all these years and I don't know if I could go through this path without their friendship and kindness My dear Negar Nahali, showed me friendship has no limit and people can be extremely kind without any expectation. Again, Georgette, my flat mate and my friend who was there during all ups and downs, listened to me and gave me comments without any bias and helped me to grow, I am grateful to her. Federica Rosselli, the strong woman in science with her rationale beside the tenderness, was always my favorite friend to go and talk with. Marco Gigante, my dearest friend in Trieste who was always present for me, who was a big support both in the lab and in life out of SISSA, I am so thankful to him.

I would like to thank Adina Drumea and Maris Skujevskis, two loving friends who tried to help me whenever I needed even if I didn't ask; and I definitely enjoyed their accompany.

I would like to thank Iga Nowak, Indrajeet Patil, Laura Babcock, Ana Laura Diez Martini and Giovanni Novembre, all the caring people who became my dear friends from the first days SISSA in the first year students' office. Those days are always bright in my mind.

There were many friends in Trieste who were very dear to me during these years and I enjoyed their accompanies; I would like to thank them all, Sahar Pirmoradian, Alireza Alemi, Fahime Baftizadeh, Andrea Perez-Villa, Julia Franzoi, Vladimir Durdević, Sebastian Reinartz, Natalia Grion, Mozhdeh Golkar, Melika Golkar, Elaheh Ghorbani, Ina Bisha, Antonio Sciarappa, Sadaf Hosseini, Matthieu Pasquet, Juan Manuel Carmona Loaiza, Alessio Isaja, Alessio Ansuini, Alessandro Di Filippo, Amir Joudaki, Fló Ana, Yamil Vidal Dos Santos, Ben Von Harling, Paola Mengotti and Jacopo Rigosa.

I am whole-heartedly grateful to L.D who believed in me, who changed my view of the life, and without that insight I couldn't have come this far in my life.

Last but not least are my dear family members. I would like to thank my parents who always had faith in me and provided me with great support through all my studies as they had promised to help their children to study as long as they want. Also I am grateful to my sister and brother, Nazli and AliReza, for their love and support throughout my life. My life without them would have no meaning. My dear brother-in-law, Mehdi Fardmanesh helped me with all his knowledge and experience in life and science and I am grateful to him.

For sure there were many more people who influenced my life and studies, my teachers and professors in Iran, my friends in Medical Students' Research Committee, and many more that I cannot name them all but I am thankful to all of them.

Abstract

A wide variety of cognitive abilities are dependent on a functional working memory (WM) system. Many attempts have been made to understand its underlying mechanism and the areas that subserve it. In the setting of tactile working memory task, two noisy vibratory stimuli separated by a delay, were applied on rats whiskers and rats had to compare the σ of the $Stim_1$ and $Stim_2$ to make a two-forced choice decision (Fassihi, Akrami et al. 2014). More precisely, in order to solve the task, the rats needed to perceive σ_1, keep its trace in memory during delay, perceive σ_2, compare σ_2 to the trace of σ_1 and choose an action based on this comparison.

Through multi-electrode recordings, we separately explored the activity of two brain areas, SII and hippocampus, to unravel their engagement across different epochs of the parametric working memory task.

In rats performing the tactile WM task, a high percentage of SII neurons in our sample showed sensory coding of the stimulus during its presentation. This activity tended to encode the comparison rule late in the presentation of the second stimulus and during the post-stimulus delay, indicating that both $Stim_1$ and $Stim_2$ affected the neuronal firing at this epoch.

In the hippocampus of rats, place coding was prevalent among the neurons, as expected by the cognitive map theory. In contrast to SII, in the hippocampal population sensory coding was not observed. However in the hippocampus, we identified neurons with choice-correlated activity during the post-stimulus delay and therefore both the σ_1 and σ_2 were factors affecting neuronal response. In conclusion,

sensory coding was mainly observed in SII while choice related activity was observed in both areas.

Table of Contents

List of Tables

List of Figures

1 Introduction

Working memory is the capacity to keep information in memory for use in the near future, information that is commonly discarded when no longer required (Cowan, 2008). Many of our daily operations rely on working memory; keeping sentences in a dialogue as one reads a novel or keeping a phone number accessible from the moment one looks it up until it can be dialed, all require working memory. Any working memory operation requires the brain to initially code the information, keep it for a brief period of time, and use it in a command. Working memory in humans has been under investigation from different perspectives, from the healthy to the diseased brain as well as across a wide variety of cognitive abilities. In the attempt to provide a theory for working memory in the intact brain, Baddeley proposed a model that consists of 3 components: phonological loop, visuospatial sketchpad and central executive (Baddeley, 1992). Attentional control through the central executive coordinates the integration of information between the two other subsystems. On the path to explore this model, several studies confirmed that this limited-capacity system provides the essential substrate for a wide range of cognitive activities such as learning (e.g., reading skills) (Alloway and Alloway, 2010), attention (Fukuda and Vogel, 2009; McCabe et al. 2010) and the ability to control the information from the environment. Additionally, insight has been obtained from working memory deficits in patients with Alzheimer's disease (Huntley and Howard, 2010) or patients with frontal lobe pathology, such as anterior cerebral artery infarction or traumatic brain injury (Milner, 1982; Eslinger and Damasio, 1985; McDowell et al., 1997; Kane and Engle, 2002). Working memory impairment in these conditions leads to poor performance not only in complex actions but also in simple daily tasks. Therefore,

many attempts have been made to understand its underlying mechanism and the areas that subserve it. However, to reach an understanding of working memory, it is crucial to note that memory is formed by traces and it is distributed across multiple brain regions. In humans these traces have been revealed using different behavioral and imaging techniques (Preuschhof al., 2006; Kaas et al. 2007).

There are inherent constraints in the current human neuroimaging techniques, including limited spatial and temporal resolution (Menon and Kim, 1999; Cannestra et al., 2001; Stelzer et al., 2014). Ethical issues, of course, make it difficult to investigate the substrate of working memory at the level of precise spiking activity in humans. Fortunately, complementary studies in other species can bridge this gap. Animal studies can provide cross-species comparisons (Carruthers, 2013) and furnish observations with the resolution of a single neuron. At present, primates (Hernandez et al., 1997; Pesaran et al., 2002), rodents (Wood et al., 1999, Fassihi, Akrami et al., 2014), pigeons (Diekamp, et al., 2002) and crows (Veit et al., 2014) have been shown to have working memory during selected sensory tasks.

In 1936, Jacobson reported a severe impairment in performance in a delayed-response task in rhesus monkeys with bilateral prefrontal lesions (Jacobsen, 1936). Following this seminal work, the delayed-response task was used in subsequent studies to examine the function of prefrontal cortex and short-term memory. Chronic recording of activity of single-neurons in awake and behaving monkeys became feasible with a method developed by Evarts (Evarts, 1968), which proved invaluable to the expanse of classical working memory studies. Using chronic recordings, the first “memory cells” in primates was discovered by Fuster and Alexander as animals performed a delayed-response task (Fuster & Alexander, 1971). In these experiments, a modified version of the Wisconsin General Test Apparatus was used in which a food morsel (cue) position previously presented to the animal was subsequently hidden from sight by an opaque screen for a delay lasting up to several seconds. The animal needed to keep the information regarding the baited position during the delay to solve the task and choose the correct location. The sustained activity observed in some prefrontal neurons during the delay period was suggestive of a prefrontal cortical role in mnemonic processes.

Afterwards, the oculomotor delayed-response task (ODR) was developed (Funahashi et al., 1989). In ODR, the monkey's head was immobilized by an instrument during the task and the animal needed to keep the fixation at a central point on the monitor while a visual cue was presented at one of eight peripheral positions in the visual field. Again, the animal needed to keep the positional information of visual cue in memory for several seconds after its disappearance to be able to saccade to the correct cued position at the end of the trial. Precise control over the timing of task events and perimetric mapping of memory to targets in several positions in the visual field were the main advantages of ODR and allowed the authors to find neurons in prefrontal cortex with sustained delay-period activity only when the cue was presented in a particular position of the visual field. The authors described quantitatively the directional selectivity of the aforementioned neurons with tuning curves suggesting memory field characteristic for these neurons.

In an influential series of experiments in monkeys, Romo and colleagues investigated the neural correlates of tactile working memory and perceptual decision-making (Romo and Salinas, 2003). The design of the task allowed the investigators to separate sequential epochs: sensory coding, maintenance of information, and decision making. In this task, the monkeys were trained to discriminate two flutter vibrational stimuli, separated by a delay, that were applied on their fingertip. The monkey had to compare the frequency of the two stimuli; therefore, solving the task required them to keep the memory of the first stimulus during the delay, in order to compare it with the latter one. In these studies, Romo and colleagues studied the neuronal activity of several different brain areas while monkeys performed the task. These studies provided tremendous contribution in the comparison of activity across different brain areas during a working memory task which can be summarized as follows: there was a graded positive stimulus encoding in the primary somatosensory cortex (SI) during the presentation of both the first and second stimulus, but with little evidence of neuronal activity that could be relevant to memory maintenance during the delay (Hernández, et al., 2000). By contrast, during the presentation of the second stimulus, the activity of a subset of neurons in the secondary somatosensory cortex (SII) was modified as a function of both the first and the second stimulus, suggesting that SII may be involved in the combination of the current information with the memory of the preceding stimulus; moreover, both positive and negative coding was observed in

SII sample of neurons, which was different from the positive coding in area SI (Romo et al., 2002). The sustained activity during the delay in the prefrontal cortex (PFC) relates these two findings as a possible mechanism for maintaining the memory. The temporal evolution of the decision was seen in the activity of the medial premotor cortex (Hernandez et al., 2002). All these observations in monkeys have indicated that highly-distributed processes that engage different brain areas underlie working memory and its consequent decision making (Romo and Salinas 2003).

Nevertheless, there is a converging initiative to study networks in the rodent brain (Koch and Reid, 2012) both for cross-species comparisons and the possibility of studying circuit analysis with invasive tools. One main reason is the feasibility of recent methods of optogenetics (Boyden et al., 2005) that enables neuroscientists to control well-defined events within specific cells of living tissue even in a behaving animal. This control permits studies with an attempt to explore the causal effect of certain neuronal populations on a specific event or task. In rodents, different paradigms have been used to investigate working memory, including delayed alternation (Wood et al., 2000), the radial arm maze (Olton and Samuelson, 1976; Olton et al, 1979), spontaneous exploration (Ennaceur and Delacour, 1988) and delayed nonmatching-to-sample (DNMS) task (Rothblat and Hayes, 1987). However, there are challenges accompanying these paradigms, including postural mediation of responses (changing body posture as a means to maintain the decision during the delayed response) and the difficulty in assessing the precise content of the encoded memory (Dudchenko, 2004). These shortcomings make it necessary to develop a different approach to study working memory. With a design adapted from the flutter discrimination task in monkeys, Fassihi and colleagues established a tactile delayed-comparison task to study working memory in rats, which comprises two main advantages: first, a parametrically-defined stimulus space as the basis of the memory to be kept during the delay, and second, the memory of the first stimulus is not adequate for the decision, which gives the possibility of studying the memory independent of the consequent decision and any postural cues during the delay (Fassihi, Akrami et al., 2014). The well-separated epochs of the task dissociate encoding, maintenance and manipulation of the sensory information. In order to figure out the role of different brain areas in the working memory network in rats, our colleagues in the SISSA laboratory have investigated the primary sensory cortex

(Fassihi, 2012; Esmaeili, 2014), prefrontal cortex (Esmaeili, 2014) and medial premotor cortex (unpub. observ.). As expected, primary sensory cortex encodes the stimulus, while stimulus traces have been observed during the delay period in the prefrontal cortex and premotor cortex. Moreover; decision-related activity is evident in the neural activity in the premotor cortex. However, the entire scheme of the working memory network in rodents is not yet understood.

It is plausible that a working memory substrate could eventually form long-term memory and be stored for remote retrieval. In humans, the medial temporal lobe and the hippocampus have traditionally been considered necessary to store information into long-term representations (Scoville and Milner, 1957; Burgess et al., 2002). Therefore, one could expect hippocampal involvement in the transition from working memory to long-term memory. In addition, there is a growing body of evidence suggesting the involvement of the hippocampus in processing of relational memory (Eichenbaum 2004) and its recruitment during working memory maintenance of novel items (Ranganath and D'Esposito, 2001; Axmacher et al., 2010; Fuentemilla et al., 2010). Even memory-predictive activity time-locked to the stimulus offset was observed in human hippocampus (Ben-Yakov and Dudai, 2011) which could potentially offer a novel hypothesis of hippocampal involvement in working memory (Leszczynski 2011). Moreover, in monkeys performing delayed-response task, hippocampal unit activity during a delay was reported, which was interpreted as experimental evidence for the involvement of hippocampus in a delayed-response task. Nonetheless, earlier findings in rodents have given rise to controversial interpretations, due partly to ambiguities in the results caused by limitations in the task design. From one aspect, cognitive mapping – a research line emanating from the discovery of place cells and their Cartesian representation of the environment (O'Keefe & Dostrovsky, 1971) – attributes to the hippocampus a role limited to spatial memory. From another aspect, engagement of the hippocampus is extended to include not only spatial but also non-spatial working memory (Woodet al., 1999), suggesting a broader function for hippocampus in rodent memory (Bunsey & Eichenbaum, 1996; Eichenbaum, 2000). All of these evidences led us to hypothesize that in rodents, the hippocampus has a wider participation in memory systems than that for which the cognitive map theory gives credit. In order to test this hypothesis and find out if the hippocampus participates widely across memory processes, we

decided to measure the hippocampal contribution to memory in the short term in the setting of a delayed-tactile-comparison task.

In rodents, SII lies lateral and anterior to SI; and receives direct input of whisker system form ventral posterolateral thalamic nucleus (Pierret, et al., 2000). There is a debate on the function of SII in rodents as participation of SII differs according to the behavioral task (Chen et al., 2013). Simultaneous recordings from SI and SII in rats discriminating texture plates (Zuo et al., 2015) have provided comparative results on perceptual and choice-related activity in these areas. The authors showed that rat's decision was more directly connected with SII than SI (Safaai et al., 2014). Top-down signaling from SII to SI in mice was also shown to be correlated with animal choice (Yang et al. 2016). In the setting of working memory in rodents, it is still unknown in which brain area the comparison of the two stimuli takes place. Considering the working memory network in monkeys (Romo and Salinas, 2003) and supposing similarities with rats, one possible candidate area for this manipulation of past and current information to make the comparison is the secondary somatosensory cortex (SII). Hence, in a separate group of rats, we have investigated neuronal activity in the whisker-related secondary somatosensory cortex as they performed the delayed comparison task involving vibrational parametric working memory.

2 METHODS

2.1 Experimental Design

The aim of this project was to train Wistar rats in a working memory task with tactile vibratory stimuli and then record from the hippocampus or secondary somatosensory cortex (SII) (one area in each rat) to explore neuronal activity in relation to the task parameters. Fassihi and colleagues had already established the tactile delayed-comparison task to study working memory in rats which we used in this project (Fassihi et al., 2014).

In the tactile working memory task, the animal is required to compare two vibrations that are separated by a varying delay. The stimuli are applied to the whiskers (macrovibrissae). At the end of each trial, the rat is rewarded for a correct decision (see Figure 2.1).

The main steps for a rat to perform the task and make the desired decision are as follows:

1. Receive the first stimulus
2. Keep the first stimulus in memory during the delay period
3. Receive the second stimulus
4. Compare the first and second stimuli
5. Make the decision based on the comparison between the amplitude of the two vibrations.

However, additional cues were used indicating the start and end of a trial, as well as reward delivery, in order to make it more comprehensible for the animal. These will be explained shortly after.

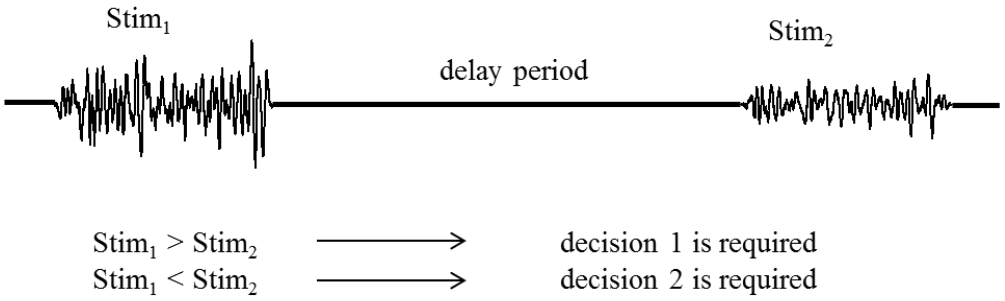

Figure 2.1. Schematic illustration of the tactile working memory task. The rat has to attend to two stimuli that are applied on its whiskers and compare them. If the first one is greater in amplitude, one decision is correct while in the case of greater amplitude for second stimuli, another decision is desired to receive the reward.

The experimental setup and training procedures had already been developed for this task (Fassihi et al., 2014) as described in details later. The setup was a Plexiglass chamber with a central hole through which the rat received the stimuli and two lateral licking ports for reward delivery (as shown schematically in Figure 2.2). In each trial, turning to one of the two sides of the maze was considered as the correct choice based on the associated rule.

A shaker motor (type 4808; Bruel and Kjaer) with maximum of 12.7 mm peak-to-peak displacement was put outside the maze to generate the stimuli. The shaker motor was placed on its flank in order to produce vibration movements in the horizontal dimension with respect to the head of the rat. A 20 by 30-mm plate was attached to the diaphragm of the shaker. This plate delivered the stimulus to the whiskers of the rat.

At the start of each trial, the rat had to approach the stimulus delivery port and keep its head fixed. The rat put the nose in the nose poke sensor. The nose poke sensor, which is composed of a diode-photodiode pair, detected the presence of the nose in order to start the trial. This sensor had a maximum buffer of 200 ms, thus head retraction lasting less than 200 ms (micro movement) was ignored; longer lasting retraction of the nose from the nose poke would lead to an early withdrawal from the

trial and a new trial needed to be initialized. This required the rat to attend to the stimuli with little movement of the head to receive the whole duration of stimuli. Once the rat put his nose in the nose poke, the plate would contact the whiskers of the rat. This plate was covered by a double-sided adhesive so that it adhered slightly to the whiskers as it moved back and forth. In this way, all movement of the plate was transferred to the whisker which was already shown (Fassihi, Akrami et al. 2014).

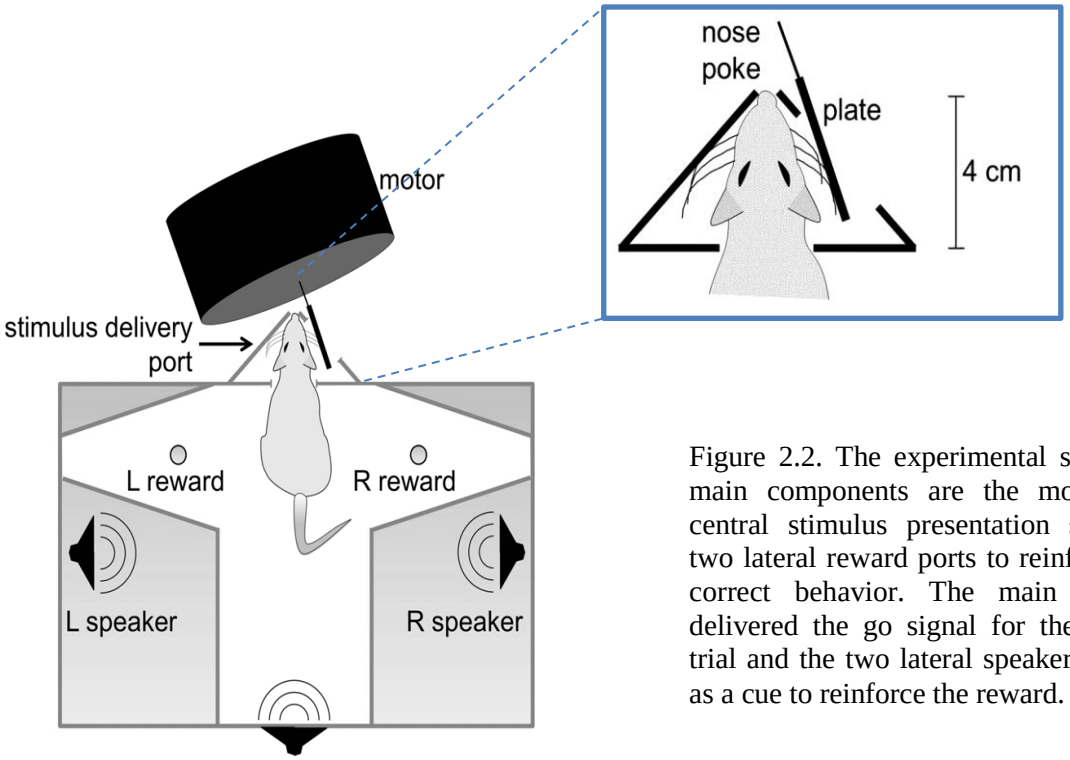

Figure 2.2. The experimental setup. Its main components are the motor, the central stimulus presentation site and two lateral reward ports to reinforce the correct behavior. The main speaker delivered the go signal for the end of trial and the two lateral speakers served as a cue to reinforce the reward.

The design of the trial is shown in the schematic Figure 2.3.

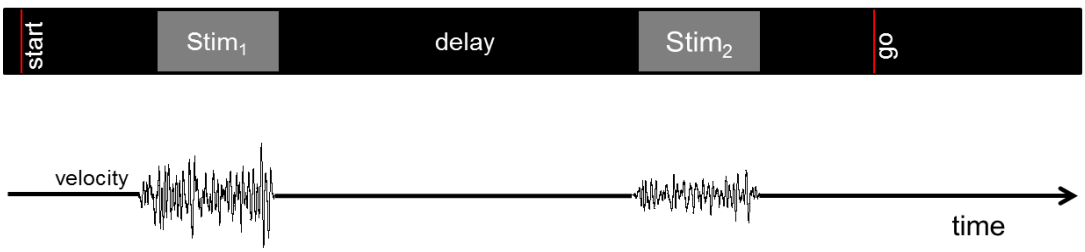

Figure 2.3. Timeline of a trial composed of different epochs with well-defined boundaries.

A trial was composed of pre-stimulus delay (500 ms), first stimulus ($Stim_1$; 600 ms), delay period (2000 ms was the delay for all rats except one, for which delays of 3500, 5000 and 6000 ms were also used), second stimulus ($Stim_2$; 600 ms), post-stimulus delay (600 ms) and go signal. Pre- and post-stimulus delays were designed to make sure that the rat received the entire stimuli and did not withdraw before the end of trial. The auditory go signal was a cue for the rat to turn to either the right or left arm of the maze.

Each stimulus was a sequence of velocity values randomly taken from a normal distribution with mean 0 and standard deviation denoted by σ. The noise sequence was low-pass filtered using a Butterworth filter with 150 Hz cutoff. Greater σ is perceived by human subjects, and presumably by rats, as a "more intense" or "stronger" stimulus. From now on, σ_1 denotes the σ value for the first stimulus and σ_2 that of the second stimulus (see Figure 2.4).

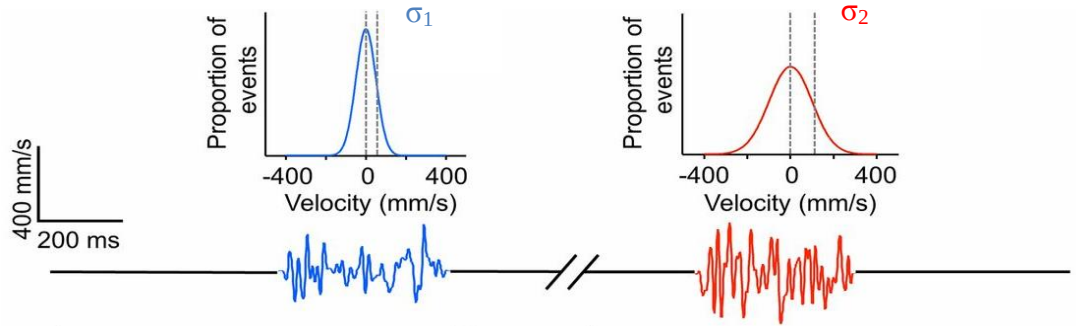

Figure 2.4. The stimuli consisted of irregular noisy vibrations randomly taken from a normal distribution.

The reward rule was based on the comparative σ values of the first and second stimulus. In total, 4 rats were included for the recordings in the behaving animal project. The rule for each rat was as follows:

For rats Ar22 and ShT2, a turn to the right was required if σ_1 was greater in amplitude in comparison with σ_2 and a turn to the left if σ_2 was greater. For rats Ar26 and Ve15, the rule was reversed for right and left arms (Table 2.1).

It was already shown that in well-trained rats, active whisking is suppressed from nose-poke entry to exit (Fassihi et al., 2014), which means that the sensorimotor system enters a "receptive sensing" mode of operation (Prescott et al., 2011, Diamond and Arabzadeh, 2013).

Table 2.1. The rule for each of the subject rats and the recording area in the brain.

Rat ID	$\sigma_1 > \sigma_2$	$\sigma_1 < \sigma_2$	Recording area
Ar22	Right	Left	Hippocampus
Ar26	Left	Right	Hippocampus
Ve15	Left	Right	Hippocampus
ShT2	Right	Left	SII

To ensure that the rats performed a working memory operation, we introduced variability into both stimuli to maintain attention. If the first stimulus is kept constant across all trials, the rat may ignore it and simply set a threshold for the second stimulus (like in a reference memory task). The same is possible if only the first stimulus varies while the second stimulus is kept constant across trials. However, our aim was for rats to attend to both stimuli and compare σ_2 and σ_1. To overcome this difficulty, a stimulus generalization matrix (SGM) adapted from Romo and colleagues, was introduced (Hernandez, Salinas et al. 1997, Romo, Brody et al. 1999). In the SGM, stimuli span a wide range of σ values. As each stimulus could appear in either position, the rat had to attend to both stimuli. However, we wanted to make sure that all pairs were in the same range of difficulty for the rat. Like binary discrimination tasks based on comparing a certain parameter for both stimuli, the difference between the two stimuli characterizes the difficulty of the task. Here, the σ of each of the two stimuli was used to define an index for quantifying the difficulty of the task. This index, called standard deviation index (SDI), was computed as follows:

$$\mathrm{SDI} = \frac{\sigma 2 - \sigma 1}{\sigma 2 + \sigma 1}$$

The logic of the SDI is based in Weber's law (Weber 1996), signifying that for lower ranges of stimuli, an absolute smaller difference is detectable whereas detecting the difference between stimuli in greater range requires greater absolute difference. Lower SDI indicates an increase in the difficulty of the task as the difference between stimuli is smaller.

The SDI of the stimuli in the task for the current experiment was set to 0.35 across all trials for all rats (except for sht2 which had a more difficult SDI of 0.3 since we

wanted to explore the sensory coding of the stimulus in area SII). The range of the stimuli σ values was set from 20 to 160 mm/s. As presented in Figure 2.5, we chose the stimuli σ values according to a fixed SDI; and on a logarithmic scale the σ values were evenly distributed.

The diagonal line in the SGM figure indicates the potential case of $\sigma_1 = \sigma_2$, which is not presented in the working memory paradigm and is just a boundary for decision category; all stimulus pairs on one side of the diagonal were associated with the same decision action. The rat had to execute a direct comparison between the two stimuli on each trial, since neither the first nor the second stimulus alone contained sufficient information to perform the task.

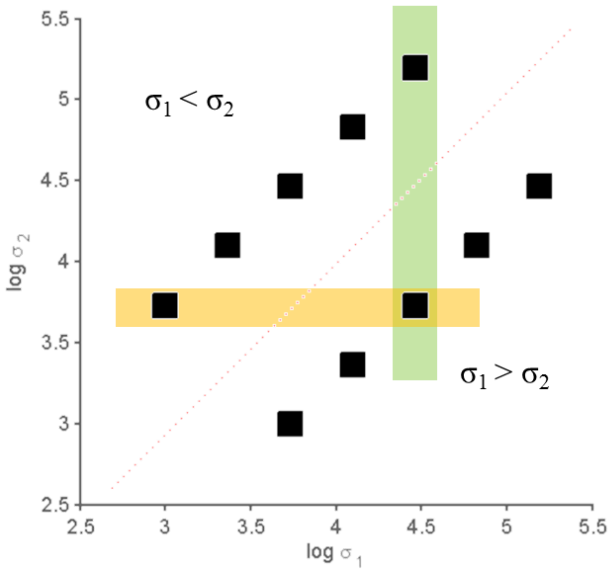

Figure 2.5. Using the same SDI to create stimulus pairs enabled us to have same relative difficulty across all pairs. The figure shows two decision categories according to the two σ values with the middle red line as the hypothetical boundary. Two different trial pairs that require different decisions can share the same value for either the first or second stimulus. This promotes attention to both stimuli.

The experiment was controlled using Labview software (National Instruments). Labview software was communicated to a computer and through the National Instrument card it was connected to the sensors and the shaker motor of the maze.

2.2 Training

As already explained by Fassihi and colleagues, the training of the animals for performing the working memory task consisted of five different stages and took 5-6 months up to one year depending on the learning rate of each rat (Fassihi et al., 2014).

Stage 1. In the first stage, the animal was handled and petted for half an hour per day for 10 days. From this stage onward, to motivate the rats to learn the task, a water restriction schedule was implemented, whereby the rat collected rewards in the apparatus and was given ad libitum access to water after each session. For each correct action of the animal, through all training and also recording sessions, a few drops of pear juice were delivered through the reward ports to the rat. The reward solution consisted of one part pear juice diluted in two parts water.

Stage 2. Nose poke and reward collection. After handling, the rat was put in the setup to explore it for the first time. Reward was then delivered to the reward spouts as soon as the rat approached it. In this way, the rat learned the reward spouts. During this stage, in the maze simultaneously with the reward delivery, a reward sound consisting of a train of 5 clicks was played from a lateral speaker positioned at the same side of reward delivery. When the animal learned the concept of reward spouts, its attention was directed manually towards the stimulus delivery port with a plastic pipette containing some drops of water. At this stage, as soon as the animal put its snout inside the nose poke, the go signal (a 200 ms 5-KHz acoustic signal) was played through the speaker and immediately the reward was delivered randomly to the right or left spout. An infrared diode/photo diode pair was used as the sensor for detection of the presence of the rat inside the nose poke. After a few trials, most rats learn the sequence of three actions to get the reward: positioning snout in the nose poke, attending the go cue and withdrawing towards the baited reward spout. After two to three sessions of this stage, most rats showed the stereotypical behavior of nose poke entry and withdrawal after the go cue to collect the reward. When rats showed at least 100 repetitions of this behavior per session, they moved to the next stage.

Stage 3. Training to wait for the go cue. Having learned the nose poke and reward delivery association, rats moved to the next stage of training which required longer

waiting time in the nose poke for the go cue. This waiting time for the go cue increased gradually across trials and days up to 6 seconds. Moreover, a blue LED was placed above the nose poke which was turned off as soon as the animal positioned the nose correctly inside the nose poke sensor. This was used as feedback to the rat for correct positioning of the nose and the start of the trial. Reward collection terminated the course of a trial and the blue LED illuminated again signaling that the rat may return to the nose poke to start the next trial. During this stage, a buffer was used for snout movement detection. The rat had to maintain the head movement in the nose poke below this buffer; otherwise, it was considered as an incorrect withdrawal and no reward was provided. Meanwhile, with the increase of the waiting time, the buffer threshold for an acceptable level of head movement was gradually reduced to make sure the rat kept his head fixed in the stimulus delivery port. The rat had to reach high performance of at least 90% to move to the next stage (less than 10% of 6 second trials could be withdrawn prematurely).

Stage 4. Introduction of tactile stimuli. At this stage, when the rat positioned its snout after a pre-stimulus delay, tactile stimuli was delivered as well. At the beginning of this stage the amplitude of the vibration was set to a minimum, not to frighten the rat. In the first session of this stage, the duration of the stimulus was gradually increased across trials to reach 600 ms. The amplitude of the stimulus was then gradually increased. One important issue in this stage is the task rule and reward association. It means that after the go cue, the reward was delivered passively on the correct side with respect to the rule for the rat under training. As previously mentioned, the rule could be one of the two following sets: $\sigma_1 > \sigma_2$ associated with the right side and $\sigma_2 > \sigma_1$ associated with the left side for reward delivery, or the reverse. Therefore, at this stage, the goal was to familiarize the rat with the association rule of the task, hence the reward was delivered passively and made available in the spout until the rat approached it. The reward target cue was played on the corresponding site until the animal received the reward. If the rat went towards the incorrect site at this stage, it still had the chance to get the reward at the correct spout (error remediation protocol). This stage lasted for up to 20 sessions for each rat. Provided that the incorrect withdrawal rate was less than 10% across all trials, the rat could move to the next stage for active choice of the reward site.

Stage 5. Implementation of the stimulus comparison rule. At this stage, after the go cue signal, the rat was required to choose one arm of the maze actively. If the chosen arm was in agreement with the correct stimuli discrimination, then the reward was delivered at the corresponding spout and the reward sound simultaneously played to reinforce. Otherwise, the trial terminated with some timeout punishment. During timeout, the blue LED of the nose poke was kept turned off as a signal that the start of the new trial was postponed due to an incorrect choice. The SDIs of the stimuli were manipulated in such a way as to make the comparison easier at this stage. The SDI was changed progressively to a more difficult one across sessions. Performance needed to be constantly above 70 percent for a rat to advance to the final training SDI (SDI= 0.25) and thereafter be included for the surgery and electrode implantation. Although SDI was set to 0.3 and 0.35 for recording sessions, the rats were trained with the most difficult SDI prior to the surgery because the post-surgery performance of a rat might decrease; a rat was expected to perform almost the same with an easier SDI after surgery.

As there were 3 almost identical setups for training and only one of the setups was provided for recording, each rat, before undergoing the implant, was moved to the recording setup. The rats were trained for about one week in the recording setup with the same pre-surgery parameters.

2.3 Surgery

In this project both chronic and acute surgeries were performed. In a chronic surgery a microwire array was implanted in the brain of a trained rat; by contrast in an acute surgery an implant was made in the brain of a naïve rat to record neuronal activity in the anesthetized rat. Although the main procedures are similar the differences will be considered in greater detail below.

2.3.1. Chronic Implant via Stereotaxic Surgery

Once the performance of the rat was appropriate for recording, the rat underwent a surgery for chronic electrode implantation. The rats had access to water ad libitum the day before surgery. All the surgical instruments and the materials needed were sterilized. The area of the surgery was cleaned and covered with a sterile pad. The rats underwent surgery with general anesthesia via inhalant anesthetic Isoflurane (concentration of 2.5% for anesthesia induction and craniotomy, 1.5% for maintenance and 1% for cement coverage) delivered through a snout mask. For the surgery, the absence of pain reflex was confirmed by toe pinch to make sure of the depth of anesthesia. During the whole surgery, the rat was kept at proper body temperature using a thermostat regulated heating pad (37-37.3 °C). Before starting the incision, the animal hair was shaved off from the ears to just in between the eyes using an electrical razor. Eye lubricant drops (Epigel) were administered to the eyes. The animal was then mounted on the stereotaxic apparatus. Once the animal was placed, using a sterile scalpel, an anterior-posterior incision was made in the midline on top of the skull from lambda to just in between the eyes. The skin was then pinched off using 4 hemostat clamps to keep the incision open. The exposed area of the scalp surface was dried using cotton swabs. The underlying connective tissue that adhered to the bone was removed from the skull surface using sterile swabs, which absorbed and minimized bleeding. This step is important since the residues can grow back and reject the cement from the skull and cause disimplantation. The rest of the surgery was guided through the microscope. The bregma and lambda were marked using a sterile pencil. The distance between the bregma and interaural line in an adult male rat should be 9 mm (Paxinos, 2007) as the rat atlas coordinates are based on this size. For the rats with a different AP distance, this was taken into account for

adjusting the coordinates. The window for craniotomy was marked with pencil on the skull.

For hippocampus implant of the electrodes, the window of the craniotomy was centered at -3.5 mm anteroposterior (AP) and 3.7 mm mediolateral (ML).

For the SII implant, the center of craniotomy was located at -3 from bregma and 7 from midline (spread -1.5 to -4.5 mm on the anteroposterior axis and 6 to 8 mm on the mediolateral axis from midline).

Two screws for connection of the reference and ground wires and one for anchoring the cement were inserted in the skull. The holes for the screw were drilled cautiously using drill tip number 2 (0.39") not to cause bleeding through touching meninges. Washed and sterilized stainless steel screws were fixed deep enough the bone to anchor the cement in the skull. The reference and ground screws were placed in contralateral parietal and occipital bones, respectively.

The surface of the skull was kept wet using normal saline. The craniotomy was made cautiously using drill tip number 1 (0.37"). During the drilling, the bone residues were blown away using air flow through low pressure air pump. In addition, the areas close to sagittal and transverse sinus were avoided because they could cause extensive bleeding and complications during the surgery. The center mass bone was then removed using forceps and the exposed area of the dura was hydrated using phosphate buffered saline (PBS). After, a small hook was made from the syringe needle for duratomy. Avoiding the veins of the dura, the surface of the dura was hooked and lifted off the brain. This minimized the dimpling associated with electrode implantation. A drop of sterile ointment was then applied in the middle of craniotomy and a small drop of surgical cyanoacrylate adhesive (Histoacryl, B Braun) was applied directly to the dura at the border of the craniotomy. This procedure helped to keep the pia matter, the top layer of the brain, adherent to the overlying bone. Therefore, the surface tension prevented the brain from depression at the advancing of the electrode; this method particularly helped for arrays consisting of 32 microwires. The cleaned electrode array (16 or 32 microwires from Tucker-Davis Technologies, TDT) was then attached to the holder of insertion device (Narashige micromanipulator).

The reference and ground wires were twisted around the corresponding screws. The tip of the electrode was then manually lowered to contact the cortical surface under the microscope guide and this was considered as zero in depth. After initial penetration of cortex, the electrodes were slowly retracted for about 50 micrometers and then pushed back inside as another method to avoid dimpling (Melzer et al., 2006). The array was advanced slowly to reach the desired depth. As the electrode reached the position and neuronal signal was controlled online, the remaining exposed surface of the brain around the microwires was covered with biocompatible silicon (KwikSil, World Precision Instruments). Having dried the surface of the skull with cotton swabs, a thin layer of dental cement was administered on the top of the skull and underneath the screws. When dried, the next layer of cement was added. When the cement became thicker but before solidification, the skin was separated from the hemostats and placed carefully around the cement, not to cause stretching after the surgery. After the dental cement was completely dried, the electrode was disconnected from the recording system and the animal was removed from the apparatus.

The rats often woke in less than 5 minutes from removal of snout mask and were put back in the clean cage. Extensive care for food and water intake in the first hours after the surgery had been provided for the rat and a hot water container was kept in the cage to keep the animal warm. Local antibiotic (gentamycin 0.1%) was rubbed all around the wound for 3 days. The antibiotic enrofloxacin (Baytril; 5 mg/kg) and pain killer (Rimadil) were added to the water supply of the rat for one week and soft food was provided to make sure the rat could take enough food. The rat had access to water ad libitum during the recovery period of one week.

For one rat, custom-made movable drive (microdrives) was used to be able to record neurons in different depths across different sessions. The microdrive has an internal screw through which the rotation movement is converted to linear movement, which in turn makes it possible to change the depth of the electrode in the brain (See Figure 2.6). The electrodes used with microdrive have a ribbon connected to them to give the flexibility of changing the position of the array with respect to the ZIF-clip connector. Each full turn of the screw caused a 250-micrometer change in the depth position of electrode.

In case of movable array, some further steps were needed postoperatively to ensure that the array could move according to turns of screw. Three days after surgery, through a hole in the drive, deionized water was injected around the implanted ribbon array to dissolve the blood clot that accumulated and free the electrode to move easily down the screw, afterwards this solution was vacuumed out. The depth of the array was then changed with turning the screw prior to each recording session.

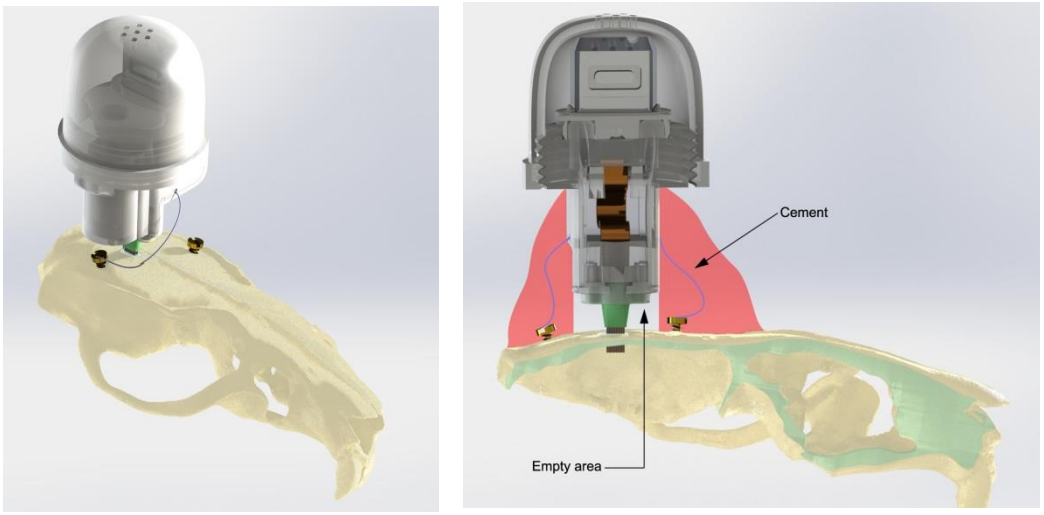

Figure 2.6. The schematic view of the microdrive that holds the movable ribbon array.

2.3.2 Mapping SII for Whiskers

In the second part of the project, we aimed at exploring neuronal activity in the whisker secondary somatosensory cortex (SII). However, since the secondary sensory cortex (SII) is located more lateral and ventral than the barrel cortex, there was a need for an appropriate coordinate system to reach the whisker-related SII cortex systematically in a repeatable manner across different rats. Therefore, we adapted a map of the secondary somatosensory cortex (Benison et al., 2007) and validated it in our acute surgeries.

For acute surgeries, mature male naïve rats were used. Craniotomy was made above the barrel cortex and the barrel cortex was mapped in two separate steps, using single electrode and the TDT array. Four barrel sites were penetrated using single electrode. The outline of the cortical arteries and veins lying over the barrel cortex makes it possible to map the barrels locations for repeatable access to the barrels with a single electrode. Whiskers were individually stimulated to figure out to which whisker stimulation the neuronal activity was most responsive.

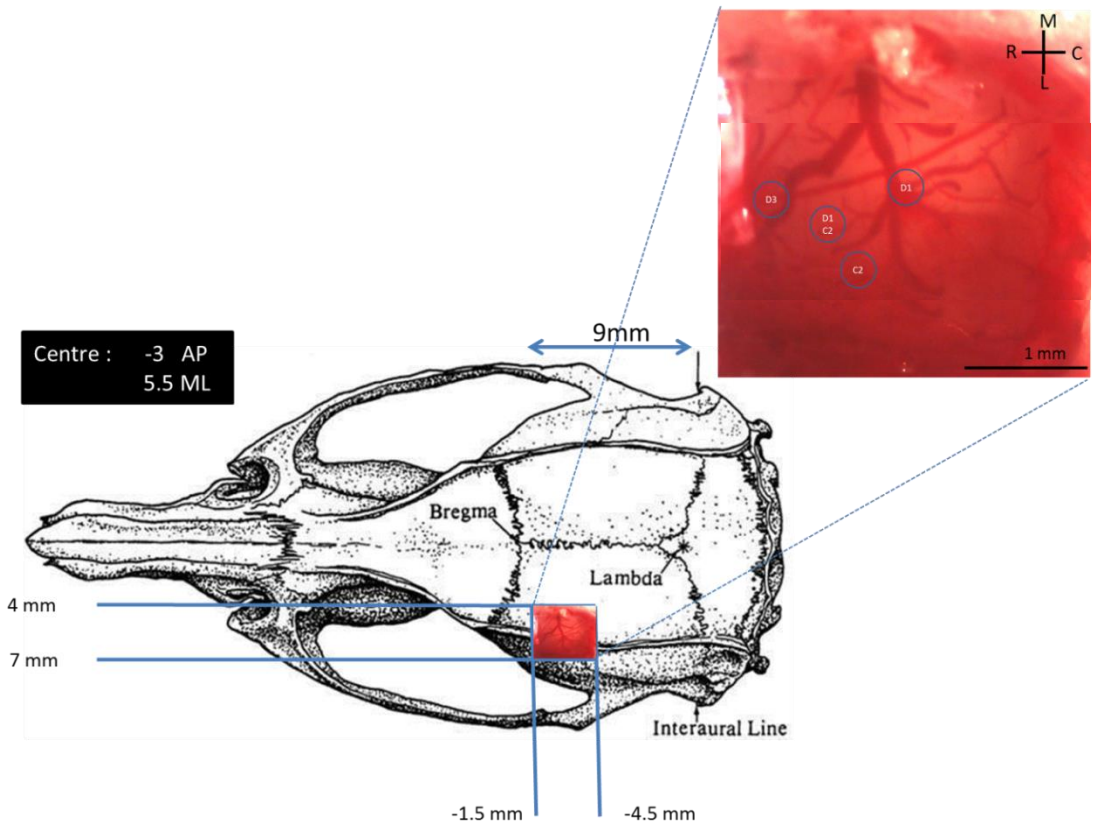

Figure 2.7. Craniotomy. The craniotomy expanded at 4 to 7 mm laterally from midline and from -1.5 to -4.5 with respect to bregma.

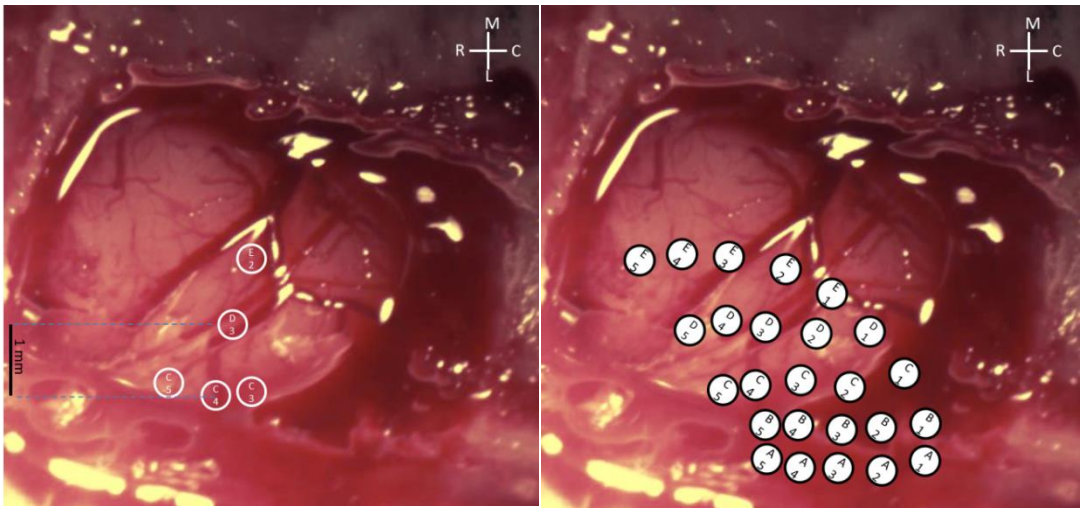

Figure 2.8. Mapping barrel cortex with single electrode. (a) Single electrode penetration sites and the relevant whisker. (b) Superimposed map of primary somatosensory cortex based on the single electrode mappings of the 5 whiskers.

The single electrode results were in agreement with the barrel cortex maps (Benison et al., 2007). Having identified the barrels, we removed the single electrode and a 16-channel TDT array was penetrated in the area where barrels were identified through stimulation.

The array was moved gradually in depth in the barrel cortex, then the whiskers were stimulated manually with a cotton swab and neural responses were recorded.

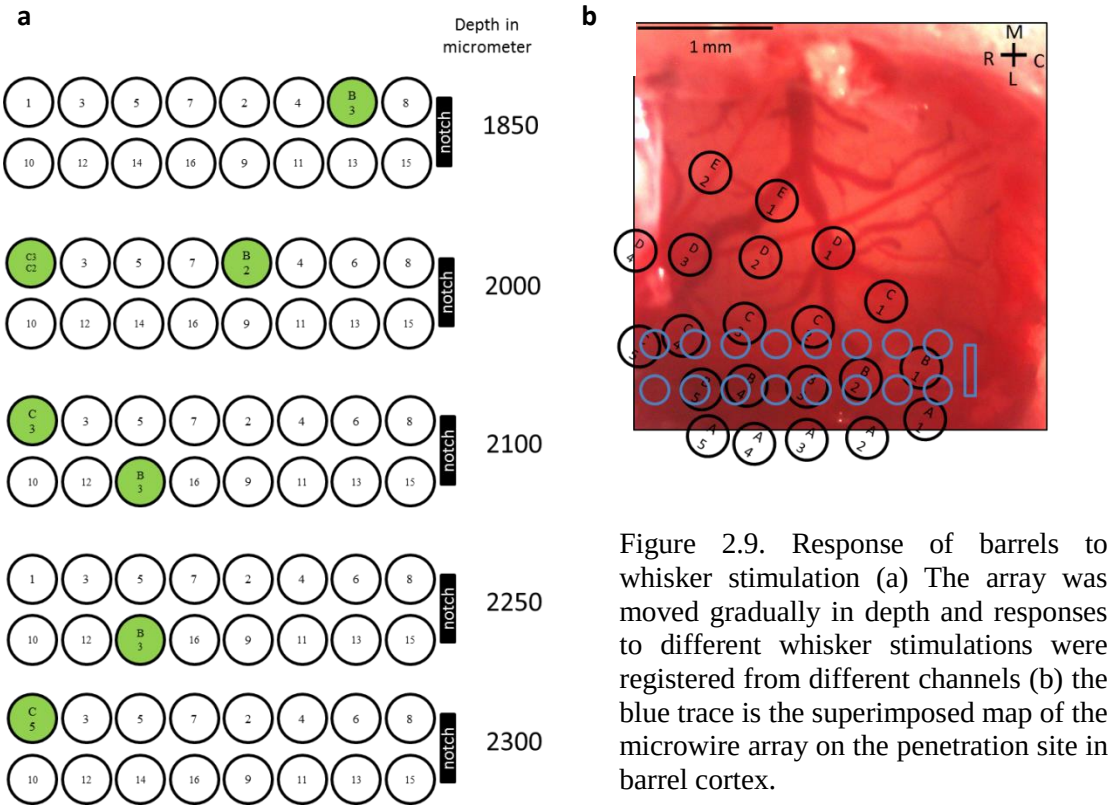

Figure 2.9. Response of barrels to whisker stimulation (a) The array was moved gradually in depth and responses to different whisker stimulations were registered from different channels (b) the blue trace is the superimposed map of the microwire array on the penetration site in barrel cortex.

The response to each whisker stimulation was monitored in different channels of the array (See Figure 2.9). Since the location of each of the channels of the TDT array was already known, it was possible to map the barrels according to these activities. Once we made sure that the maps of single electrodes and TDT array confirmed each other in the barrel cortex, we moved the TDT array deeper to reach the SII cortex.

After passing the nose area of SII, at about 2000 μm the electrodes arrived at SII for whiskers. At 2100 μm, the electrodes reached C-row whisker-related area of secondary somatosensory cortex, with the D-row-related one lying at 2200 μm. A- and B-row of whisker-related SII were located more medially, which was again in accordance with the map.

After validation of this map in 3 surgeries and the confirmation of the histology that the array reached SII, we moved to the next phase of the project and recorded in anesthetized and behaving animals with the vibrational stimuli.

Evoked responses to vibration stimuli are not yet well studied; therefore, it would be interesting both for coding of the stimuli and decoding of it according to neuronal responses. For this purpose we decided to use vibratory stimuli with varying sigma in anesthetized animal. The rats were anesthetized using urethane. A 16-channel TDT array was penetrated at 7 mm lateral to the midline. The array was positioned at a level of -2 to -3 mm relative to bregma.

After the array was penetrated in the whisker SII cortex, vibration stimuli were applied on the whiskers. Stimuli were delivered using a plate attached to the shaker similar to the working memory task. The plate was covered with a double sided adhesive and the whiskers were attached to the adhesive to receive all the displacements of the motor for the stimuli. It was already shown that the attached whiskers follow closely the plate movements (Fassihi, Akrami et al. 2014).

Stimuli with varying sigma values that was generated with 3 different seeds per each σ. The stimuli were composed of white noise with the length of 2 s, with the sigma value ranging from 43 to 148 mm/s (the stimuli were chosen with increasing steps of 0.1 of SDI from the smallest sigma.).
At the end of surgery, the rat was sacrificed and perfused to check the penetration site of the array

2.4 Electrophysiological Recording

The microwire array (Tucker-Davis Technologies) was comprised of 16 or 32 polyimide-insulated tungsten wires of 50 µm diameter. The specification of the array of microwires used for each rat is shown in Table 2.2.

Table 2.2. Microwire array specification.

Rat Id	Type	Number of channels	Tip angle	length (mm)	Row separation (um)	Electrode spacing (um)
Ar22	Fixed	16	60°	4.2 - 4.8	375	250
Ar26	Fixed	32	60°	4.2 - 4.8	375	175
Sht2	Fixed	16	60°	3.5	375	250
Ve15	Ribbon	32	60°	5	375	250
Naïve rats	Fixed	16	60°	2.8	375	250

The impedance of each wire was 20 kΩ, at 1 kHz, measured in saline, and around 150-200 kΩ when measured in vivo (Prasad and Sanchez, 2012). While lowering the arrays, the quality of raw signals was monitored and the detected spikes were clustered and sorted online using the OpenEx toolbox (Tucker-Davis Technologies). For the hippocampus, the fixed array was implanted at 4200 and 4800 micrometer depth as half of the microwires were 4.2 and the other half were 4.8 mm long. This allowed us to record from two different depths in the hippocampus. For SII recordings, the depth of implant was 2500 µm. After passing through a unity-gain headstage, signals were transmitted through a cable to PZ2 preamplifier (Tucker-Davis Technologies). Signals were then digitized at a sampling rate of 24,414.0625 kHz and sent through an optical fiber to RZ2 amplifier (Tucker-Davis Technologies), where they were amplified and stored. Data were then analyzed offline using custom-build Matlab codes (MathWorks).

2.5. Analysis of Neuronal Data

A microelectrode can register both the fast (in the order of fraction of millisecond) and slow (as slow as a hundred milliseconds) cellular local field potential signals. Synaptic potentials are slow cellular events lasting up to 100 ms and give rise to local field potentials, which consist of continuously varying voltages in time. The fast cellular events include the action potentials which appear as spikes and last around 1ms. Spiking activity can be modeled as a point process, and, assuming that all the spike events are identical, consists of a sequence of spike times. Hence, both spiking and LFP activity are time series. Time series analysis comprises two main branches: time-domain methods and frequency-domain methods.

2.5.1 Spike Sorting

The recorded extracellular action potential of a neuron should be separated from background noise. Appropriate referencing is required to minimize the correlated and uncorrelated sources of noise. At the recording time, the data was referenced to a wire connected to the reference screw located in the skull on another area separate from the recording area to subtract out correlated sources of noise. In all the surgeries in this study, a large electrode as a stainless-steel bone screw was penetrated in the contralateral parietal bone as the main reference, with the coordinates of -6 AP and -4 ML.

This large electrode reference is helpful but there is a significant size and impedance mismatch between the reference and the recording sites on the microelectrode array when using a large reference electrode. Because of this mismatch, the representation of correlated sources of noise (such as motion artifact and 50 Hz noise) is different between the reference and the microelectrode sites; therefore, these noises are not fully removed. Moreover, since this screw reference is distal from the microelectrode site, the difference between the voltage representation of correlated sources of noise at the reference and microelectrode sites is increased. And this reference may also add some ECoG (electrocorticogram) signal at the dural surface into the recording.

In order to remove these correlated sources of noise, as a further step and usual convention, one of the microwires of the array can be set as re-reference, which is done offline. This channel activity is chosen usually according to two criteria: the

baseline noise level in it is less than 5-10 microvolts and it doesn't show any apparent spiking activity. Although this kind of re-reference matches in geometry and impedance to the other microelectrodes, it has greater impedance and may cause more thermal noise in the recording. This problem becomes worse in the case of chronic implants because impedance of the implanted electrode increases due to fibrous tissue encapsulating the array (Ludwig et al., 2006; Ludwig et al., 2009).

Having considered these issues, we decided to use another method for re-referencing our data offline in addition to the large screw reference. Eventually, we used common average reference abbreviated as CAR in this text (Ludwig et al., 2009). In this method, an average of all the recordings on every good electrode site is taken and used as a re-reference. Therefore, only the common noise on all good sites remains on the CAR (mostly the 50-Hz noise and motion aftereffect). Moreover, uncorrelated random noise (e.g. thermal noise and distal neural sources) with a zero mean is minimized in this method. Single unit activity does not appear on CAR as it is averaged (Ludwig et al., 2009).

Through the averaging process, only signal/noise that is common to all sites (correlated) remains on the CAR (50-Hz noise and motion artifact). Signal that is isolated on one site (single-unit activity) does not appear on CAR, unless the signal is so large as to dominate the average (Cooper et al., 2003; Offner, 1950; Osselton, 1965). Uncorrelated random noise (e.g., thermal noise and distal neural sources) with a zero mean is minimized through the averaging process (Ludwig et al., 2009).

As CAR, we make the re-reference as average of all good sites (as some individual sites on a microelectrode may function improperly during the chronic implants, we had to identify and remove these bad sites). For this, we computed the root mean square (RMS) of each channel. We then computed the average RMS of all the recording channels. A channel was considered good only if its RMS was between 0.3 and 2 times the average RMS of the noise floor across all of the sites on the array (Ludwig et al., 2009). This criterion removed all the bad channels which were visually evident of not functioning properly at the time of recording.

When re-referenced to CAR, the amplitude of all samples of a good site is slightly decreased since each good recording site contributes to the average calculated CAR. More precisely, the amplitude of each sample will be (n-1)/n times the original value

with n channels included in CAR (Offner, 1950; Osselton, 1965). However, the signal-to-noise ratio increases as the common sources of noise are minimized more efficiently in comparison with the traditional method of single channel re-reference. In order to illustrate this advantage provided by CAR, for one of the sample channels of recording, we have computed the noise level in the data with traditional referencing method and the CAR method. For the noise estimation, we computed the estimate of the standard deviation of the background noise (Quiroga et al., 2004) (this will be explained in more detail shortly after as it is the basis of setting the threshold of spike detection in Wave_clus software). In Table 2.3, the computed estimate of the standard deviation of noise (defined as σ_n = median {|x|/0.6745} with x as the bandpass-filtered signal) is shown. As it is clear in all of the good channels that were included in the CAR, the noise estimate is decreased compared with the traditional referencing.

Table 2.3. The difference between traditional single channel referencing and common average referencing in noise estimation. CAR in general decreased the noise estimation more than single channel reference.

Channel	Traditional Ref	CAR
1	11.56999872	9.089441295
2	8.181959675	5.444296478
6	8.809071351	5.497630508
7	7.981013654	4.974394511
10	10.93254012	8.170834325
14	8.760137356	5.814274364
17	12.83655213	10.2908932
18	10.33706613	8.426615426
19	11.46957122	8.892729005
20	10.83976594	8.920233737
21	9.565680391	6.578707326
22	9.538447683	6.540447396
24	15.31389014	13.2434577
26	9.783362079	7.030342529
29	9.455871005	8.010829635
31	9.225762385	7.645744125
32	10.56800195	7.753967879

In order to illustrate it, we have plotted samples in 10 seconds of the recording for one channel in both conditions of traditional single channel reference and CAR (See Figure 2.10).

In Figure 2.11, the samples for 2 seconds of the two methods of re-referencing are superimposed. Again, it should be mentioned that CAR affects both signal and noise, but in a way that the overall signal-to-noise ratio is improved.

As mentioned earlier, the data was collected with a sampling rate of 24,414.0625 Hz as the default of Tucker-Davis Technologies recording system. The neuronal recordings were sorted using Wave_clus2 (Quiroga et al., 2004). Wave_clus is an unsupervised algorithm that can be modified in a semi-automated manner according to the preference of the experimenter.

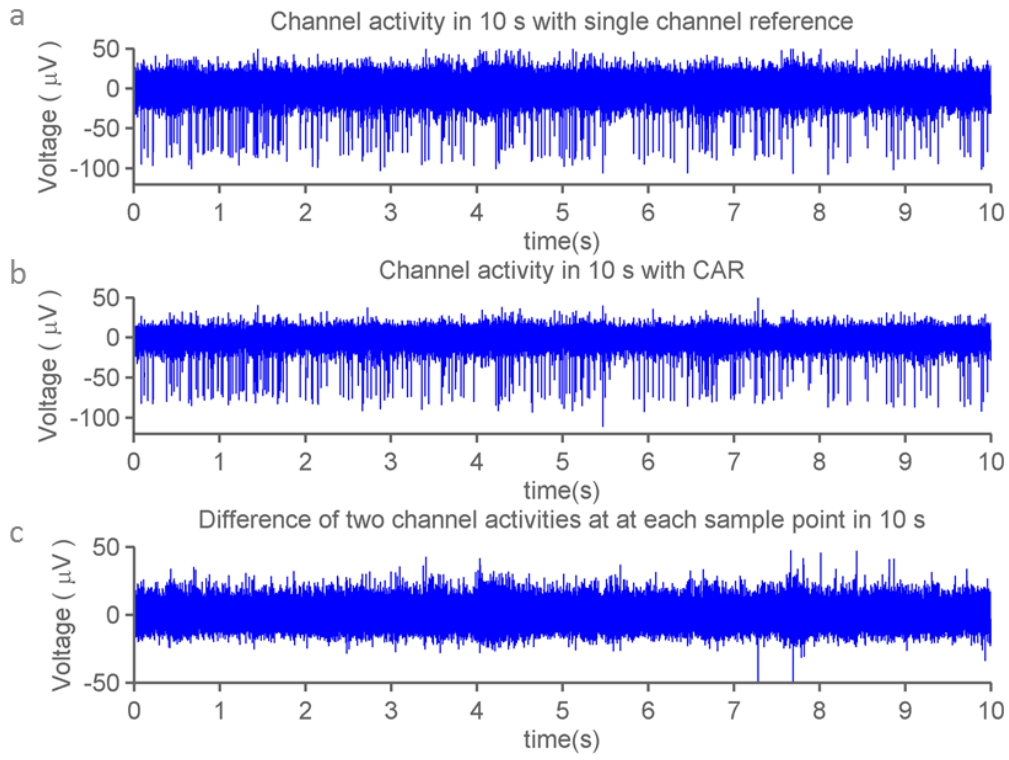

Figure 2.10. The difference between CAR and single channel reference during 10 s of recording. Same channel activity was filtered and referenced once with a single channel (a) and once with CAR (b). The difference in the electrical activity of two cases is shown in panel (c).

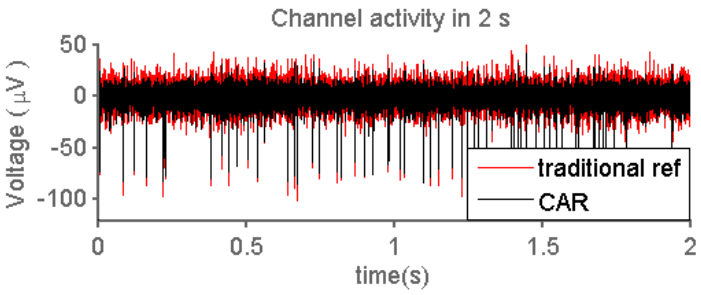

Figure 2.11. Comparing CAR with single channel reference Electrical activity referenced with CAR (black trace) is superimposed over traditional single channel reference (red trace).

After re-referencing with CAR, the data was bandpass filtered with an elliptic noncausal filter between 400 and 5000 Hz. We avoided causal filters as they can change the appearance of artifacts and make them more similar to real neural data (Quian Quiroga, 2009). Subsequently, the spikes are usually visualized on top of a background noise activity and can be detected by setting a threshold. In Wave_clus there is an automatic threshold as follows:

$thr = k^* \sigma_n$

$\sigma_n = \text{median}\{|x|/0.6745\}$

with x as the bandpass-filtered signal and σ_n as an estimate of the background noise (Quian Quiroga, 2009). The idea is that as spikes represent a small quantity in comparison with the whole sample, the median of the sample can be representative of the background noise. This eliminates the interference of high amplitude and frequent spikes from the threshold (in contrast to the shortcoming of the alternative method of choosing the standard deviation as the threshold).

In all of our data, k was set at 4 for spike detection and if it was showing threshold cutoff, we would redetect spikes with lower k of 3 (cut-off threshold can be observed in the trough amplitude histogram as will be explained later in this section). And in cases of highly noise background activity, k was set to 5 and the spikes were redetected.

For each detected spike, 64 samples (almost 2.5 ms) were saved, which included 20 samples before the peak and 44 samples after the peak. All spikes in wave_clus were aligned to their maximum. After the spikes are detected, the features of spike shapes are extracted through wavelet analysis. As wavelet is a time-scale decomposition of the signal, its coefficients are used in dimensionality reduction of the detected spikes. More specifically, the wavelet transform of each of the detected spikes is calculated

and the optimal wavelet coefficients that represent the spikes are entered as input to the next stage of clustering. As the last stage, the spikes with similar features are grouped into the same clusters using super-paramagnetic clustering (SPC). SPC doesn't assume any particular distribution for the data and groups signals based on a single parameter of temperature (Quian Quiroga, 2009). The idea of temperature comes from statistical physics and spins with different states. In a relatively high temperature of paramagnetic regime, all the spins change state independently, partitioning the data into several clusters whereas in a low temperature, the spins are in a ferromagnetic phase and thus move to another state at the same time so that all the spins fall into the same cluster. However, in a medium range of temperature (the superparamagnetic phase), only the spins that are grouped together (as they have high interaction) change their state simultaneously and therefore the clusters that group the data appear. In the case of spike sorting, each spike is treated as a spin. As mentioned earlier, in this method, there is no assumption of Gaussian distribution or nonoverlapping characteristic for spike clusters as it only works based on k-nearest neighbor interactions. As the interaction and clusters are calculated for all temperatures, one can manipulate the temperature to achieve different clusters. At this stage, we checked the output of wave_clus to check if any two clusters could be manually merged. In principle, the spikes coming from a neuron in a given electrode have a particular shape (different factors like the morphology of a neuron's dentritic tree, the distance and orientation relative to the recording microwire and properties of the extracellular medium determine the shape).

We then checked the histogram of the signal-to-noise ratio of spikes of each of the clusters. For a good unit separable from the background, we expected a distribution of SNR with a mean greater than 1. Signal was defined as the spike amplitude during 1 ms around the peak of the spike over the surrounding noise window of 2 milliseconds. Then, for each cluster, the interspike interval histogram with bins of 1 ms was generated and inspected for an absolute refractory period as an additional measure of noise rejection. For a given neuron, immediately after a spike, due to biological constraint, the neuron cannot fire another spike. Therefore, if we assume that the majority of the spikes in a cluster arise from a single unit, the spiking behavior leads to an exponentially declining tail in ISI distribution that follows a Poisson distribution. For a single unit, the refractory period of 3 milliseconds in ISI

distribution should not include a high percentage of spikes; more specifically, the ISI violation of a single unit should be less than 5% of all spikes in that cluster. This ISI violation is in fact denoting the false positive events from overlap with all other clusters in that channel. The lower this violation is for a given cluster, the more one can be sure that these signals are not contaminated with signals from other units (Hill et al., 2011). Subsequently, we checked the distribution of the peak of the spikes in each cluster. Those clusters that could potentially fall into the same group were inspected more precisely for the peak amplitude distribution. If the two clusters with similar waveforms follow the same range in the distribution, then they could be merged to make one single cluster. In Figures 2.12 - 2.14, examples of single units and the quality metrics are illustrated in panels:

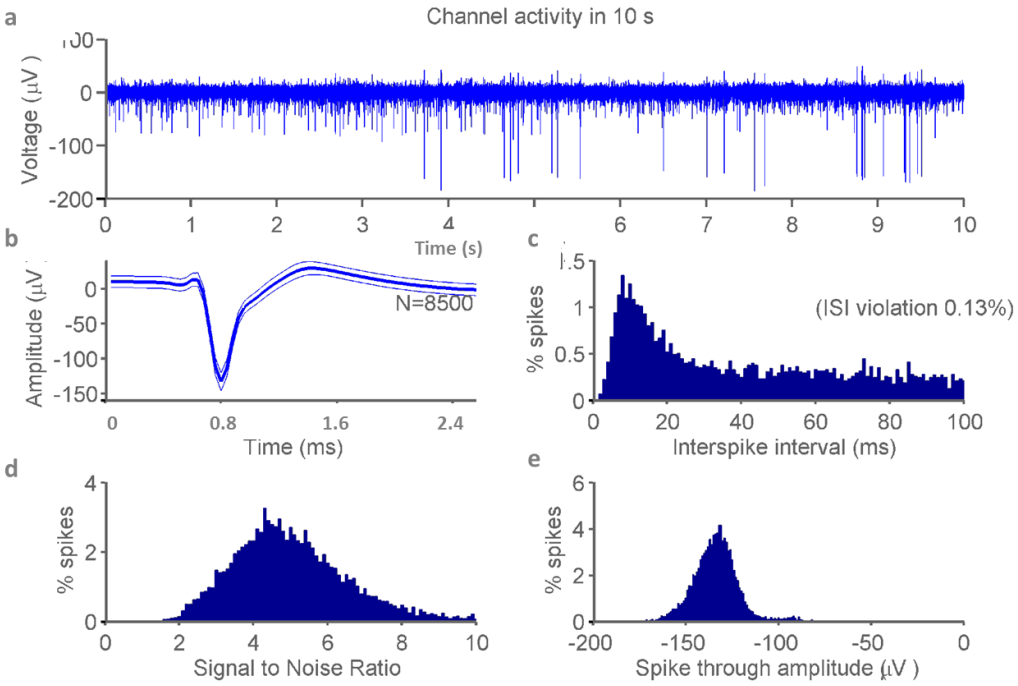

Figure 2.12 Quality metrics for an exemplar neuron. Panel (a) illustrates the activity of the channel during 10 seconds of recording. The average waveform of the neuron (+/-1standard deviation) is shown in panel (b). Panel (c) shows the ISI distribution. ISI violation is the percent of spikes that occurred in less than 3 ms from the preceding spike. Panel (d) shows the signal-to-noise (SNR) ratio distribution. The SNR for each spike is set as the ratio between the amplitude of spike and the surrounding noise. Finally, panel (e) is the distribution of the peak of the spikes.

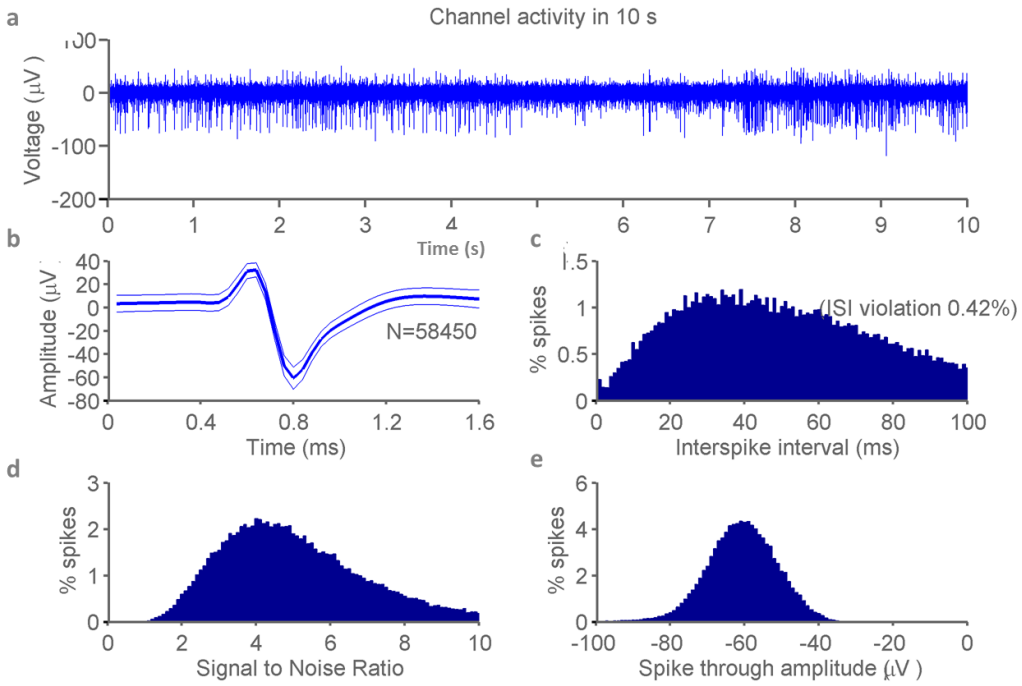

Figure 2.13 Quality metrics for an exemplar neuron. Panels are as in Figure 2.12.

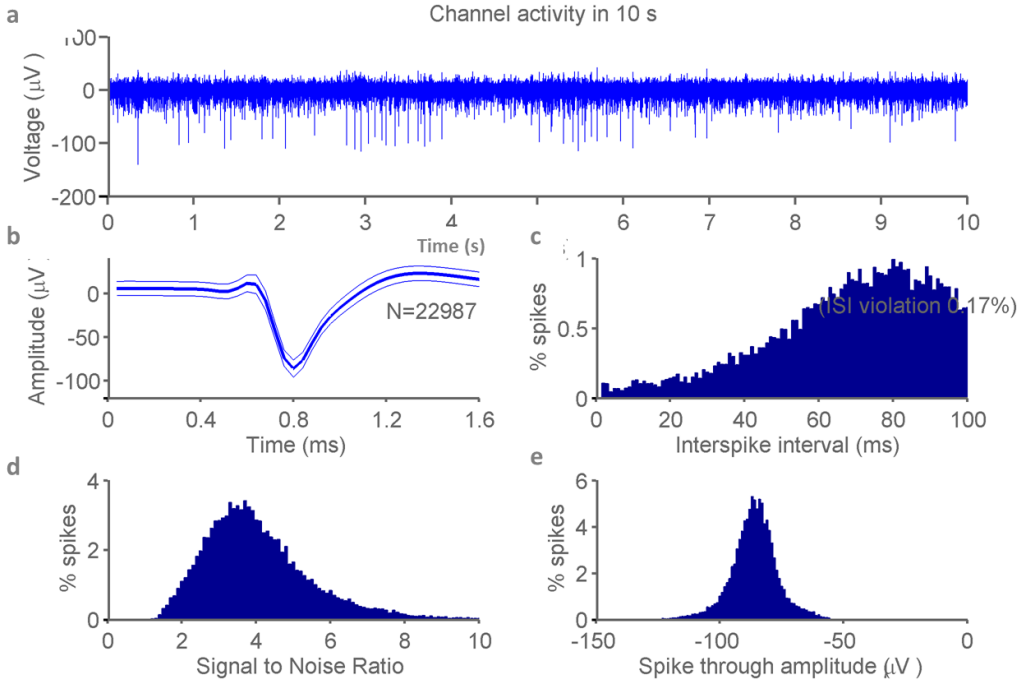

Figure 2.14 Quality metrics for an exemplar neuron. Panels are as in Figure 2.12.

2.5.2 Time-Domain Analysis:

The data were analyzed using time-domain analysis on the spike train of each neuron with the resolution of 1 ms. Data of sample neurons of SII and the hippocampus were analyzed separately applying the following method. The analysis was done without any smoothing of the spike train.

The data analysis was carried out only for trials with correct responses (except for the analysis to identify the place coding neurons). Our analysis consisted of a multi-step process. We first examined the sensory coding, decision coding and place coding activity of neurons. Next, the change in firing activity of each neuron in different epochs of the task as a function of the two stimuli was considered to investigate how the population activity was changed over epochs. Finally, the change of firing dynamics of single neurons over time was assessed.

To classify the function of neurons with respect to task epochs and parameters, a Spearman correlation between the spike count and the relevant task parameter was calculated. For this purpose, for each neuron, spikes were binned over 100-ms non-overlapping windows for each trial. The Spearman correlation between spike counts in each bin with the three following parameters was tested:

- First stimulus value (σ_1)
- Second stimulus value (σ_2)
- Comparison rule (σ_2- σ_1), as an indication of the decision of the animal

As a consequence of our binning, correlation with σ_1 was assessed in 6 bins during $Stim_1$. Any neuron which was significantly correlated with σ_1 in at least 2 bins out of 6 during the first stimulus presentation was classified as a $stim_1$-coder (this was an arbitrary definition). If we consider the chance of type one error at 0.05 (since we considered any correlation with p value less than 0.05 as significant), the chance level ($P_{stim1coder}$) for a given neuron to be classified as $stim_1$-coder merely due to statistical chance can be calculated as:

$$P_{stim1coder} = \sum_{k=2}^{6} \binom{6}{k} 0.05^k (1 - 0.05)^{6-k}$$

which is 0.03 in this case. Thus a given neuron would be expected a prior to surpass this criterion of significance with a likelihood of 0.03 by chance. Similarly,

correlation between spike count and σ_2 was calculated in 6 bins during $Stim_2$ while the correlation test between the comparison rule and spike count was performed over the 5 bins of post-stimulus delay. The neurons with significant correlation with σ_2 in at least 2 bins out of 6 of $Stim_2$ were considered $stim_2$-coders. The same calculation for the chance of a neuron being considered as $stim_2$-coder can be performed; this yields the same 0.03 of the population being considered as $stim_2$-coder as a consequence of statistical chance in our analysis.

Likewise, if a neuron's activity showed a significant correlation with the comparison rule in at least 2 bins of post stimulus delay, it was assigned to the decision-coding group. In this case, 0.02 of the population by chance could be considered as decision-coders.

The Spearman correlation between the rat's action and the spike count in the window of 1000 ms following the go cue was calculated, and cells with a spike count significantly correlated with the animal's action were classified as place coders (this analysis was performed only in the hippocampal population).

For a more general analysis in the second step, we considered the joint dependence of a neuron firing to both σ_1 and σ_2. We chose a planar function of σ_2 and σ_1 and fit the firing of neurons to it. The function was as follows:

spike count = $w_1 * \log \sigma_1 + w_2 * \log \sigma_2 + c$

The coefficients w_1 and w_2, are measures of dependence of firing counts as a function of σ_1 and σ_2 according to the above expression. Over each of the three epochs of $Stim_1$, $Stim_2$ and post-stimulus delay, the firing rate of each neuron was fit with this function. This could give us an overall view of the distribution of set of neurons along the plane of w_1 and w_2.

In order to estimate the proportion of neurons with dynamics proportional to $\sigma_2 - \sigma_1$, the firing of neurons from the start of $Stim_2$ until the end of post-stimulus delay was approximated with the following function:

Spike count = $w_{choice} * (\sigma_2 - \sigma_1) + constant$

The bin window was 200 ms and shifted in steps of 25 ms. The sliding window would give us an estimate of the choice coding during this interval.

For the acute recordings in SII, only the Spearman correlation between the 7 different sigma values and the spike count during stimulus presentation was performed.

2.5.3 LFP Analysis

In contrast to spiking activity, LFP activity is a continuous process which consists of varying voltages during time. Signal time series was transformed to the frequency domain using Fourier Transform and the power spectrum of the data was computed. The rhythmic activity in the data as a function of frequency is revealed by the power spectrum. In order to get the LFP, the raw data were bandpass filtered between 1-300 Hz offline and then down sampled with a sampling rate of 1,000 samples per second (this high sampling rate kept the analysis safe from aliasing impact).

The power spectrum ($S_{\chi\chi,j}$) of the signal is defined as:

$S_{\chi\chi,j}= (2\Delta^2/ T)\ \chi_j\ \chi_j^*$

where χ_j and χ_j^* is the Fourier transform of signal χ and its complex conjugate respectively, Δ is the sampling interval (in this case 0.001 s) and T is the total duration of recording in seconds (depending on the recording session). The $S_{\chi\chi,j}$ unit is $\mu V^2/Hz$. In signal processing, the Nyquist frequency is half of the sampling frequency, in this case 500 ($1/2\Delta$). The Nyquist frequency is the highest frequency, which can be observed in the power spectrum. Only the power spectrum within the range of 1-300 was included in the rest of the analysis. The frequency resolution is the reciprocal of the total recording duration (T) which indicated the lowest frequency difference to be resolved. In our studies, the minimum recording duration belonged to acute recording with 10 minutes duration. Therefore the frequency difference of 0.001 could be resolved in these recordings.

For the purpose of better visualization of lower amplitude rhythms, the power spectrum scale was changed to decibels. For the spectrogram of the LFP activity during trial epochs, we used Chronux_2_10 toolbox for Matlab, which performs the multitaper analysis (Bokil et al., 2010). We used the direct multitaper estimate in this case. In this method, multiple (k different) orthogonal tapers are chosen and the data are multiplied by these tapers. The choice of taper functions is made by Slepian functions (Slepian and Pollack, 1961). Slepian functions have the characteristic that for a taper length of N and bandwidth parameter W, there exist k sequences that have the energy effectively concentrated within a range [-W,W] of frequency space and k is equal to 2NW-1. These k leading Slepian functions are taken as data tapers in the

multitaper analysis and LFP data are separately multiplied by each of these tapers and afterwards the Fourier transform of it is computed. A direct multitaper estimate of the underlying process is the arithmetic average of these spectra. The variance of the estimate is reduced by 2NW. There are two main advantages for this method as problems of bias (both narrow-band and broad-band) and variance are easily overcome. The use of multitapers makes the data smoother (depending on the choice of W and N) and they can be used to increase spectral resolution.

The multitaper estimate was performed with duration of 600 ms and bandwidth 5 Hz. These tapers better captured the transients in the signal with high enough frequency resolution.

3 Results

3.1 Behavioral Results

Behavioral results for the working memory task was already reported by Fassihi and colleagues (Fassihi et al., 2014) and we could replicate their results. 4 rats were trained to perform the working memory task to reach stable performance, defined in the Methods chapter as performance consistently above 70% for a period of one week. The performance was monitored for different pairs of stimuli spanning the entire SGM.

As a new investigation in the behavior, we wanted to make sure of the independence across sessions. Independence implies that the probability of correct response should be the same across different sessions. Thus, we can assume that the performance across all sessions of a given rat should follow a binomial distribution centered at the average performance of that rat.

The probability density function of a binomial distribution is:

$F(k;n,p)= \binom{n}{k} p^k (1-p)^{n-k}$

where n is the number of trials (e.g., 100), k is the number of successes with p being the success rate of 0.72. p is the average performance across all trials of all sessions (e.g., success rate of 0.72). We calculated the performance in sessions containing at least 100 trials. For sessions with more than 100 trials, we chose randomly 100 of the trials to include in the analysis and calculated the performance across those trials. The distribution of performances of one rat across sessions is illustrated in Figure 3.1, and

it is apparent that the observed distribution adheres to a binomial distribution with success rate of 0.72. This result is consistent with the idea that the capacity of the rat did not vary slowly or systematically over time. Nonetheless, in this analysis, as the number of trials per session increased, the agreement between the binomial pdf and performances decreased, and the reason is that the rat performed fewer sessions with higher number of trials. For instance, there were only 39 sessions with 160 trials while 101 sessions included 100 trials.

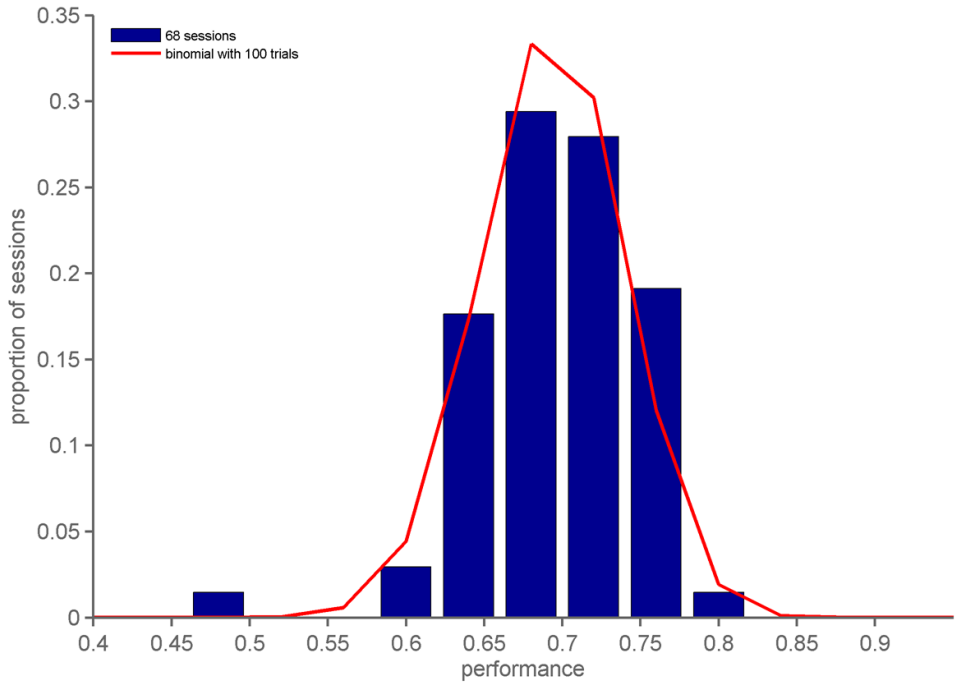

Figure 3.1. The performance of one rat (ve15) across sessions followed a binomial distribution. Histogram of performance across different sessions is shown in blue bars. Average per performance of the rat was 0.72. The red trace is the probability density function of a binomial distribution with p= 0.72 for 100 trials.

We performed the same analysis for each of the rats included in this project and the results were similar in the sense that the success rate was fairly consistent for all trials for each individual rat. Similar results for the other 3 rats, are shown in Figure A. 1 to Figure A. 3 in the appendix.

These results collectively suggest that sessions are independent (rat employs the same strategy and sensory capacity) and trials from different sessions can be pooled together.

Figure 3.2 shows the performance, as percent correct, for each stimulus pair, averaged across recording sessions for rats. The high performance across different stimulus pairs confirms that the rats were performing the working memory task in recording sessions and the performances were not dependent only on the first or second stimulus.

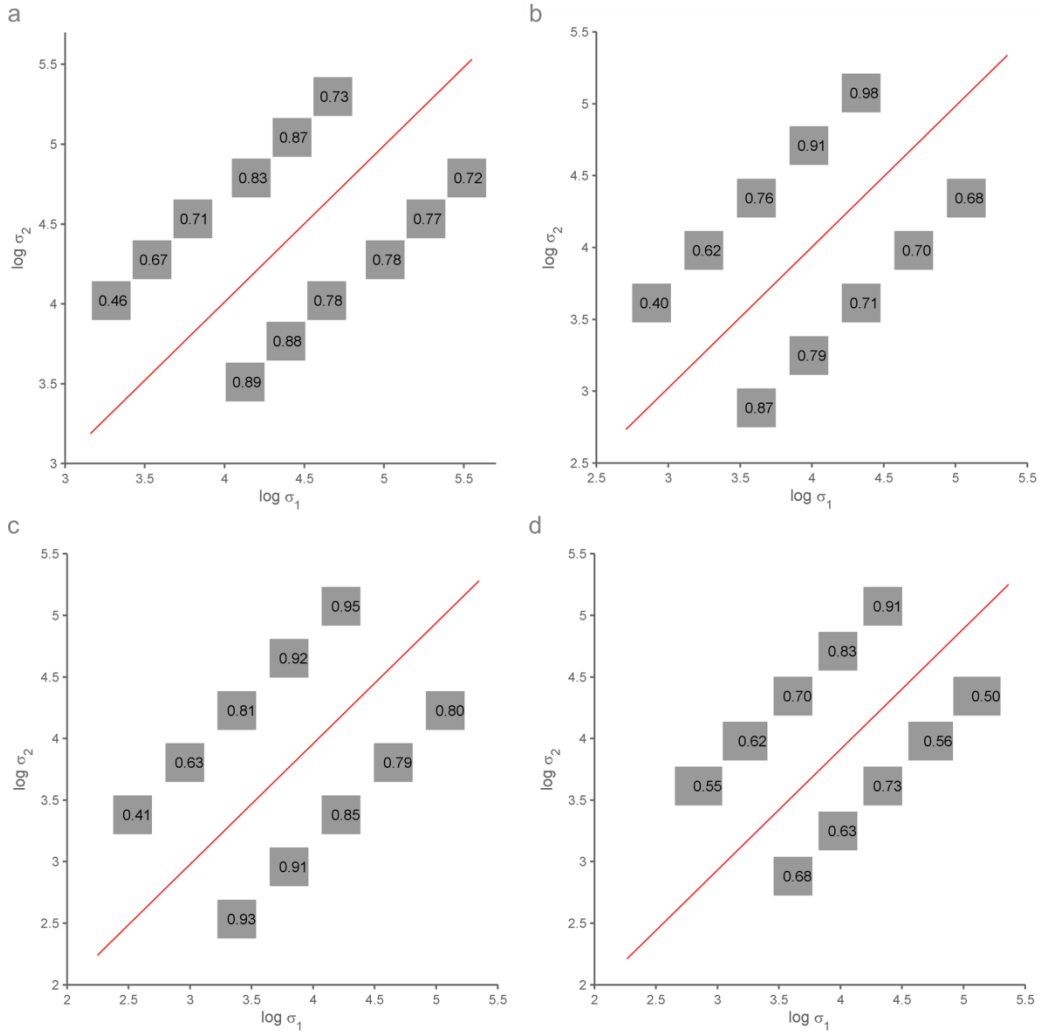

Figure 3.2. The average performance of rats for SGM design over recording sessions. The red diagonal line indicates the decision boundary. The performance of (a) ShT2 with SII implant, (b) Ve15, (c) Ar26 and (d) Ar22 with hippocampal implants over the recording sessions of each rat are shown.

In the SGM, most rats manifested a bias: they perform lower for the low-to-high stimulus pairs that have small σ values. This error has been attributed to contraction bias, a phenomenon known in psychology for more than a century (Hollingworth, 1910; Fassihi et al., 2014). According to contraction bias, when two stimuli are presented sequentially, error occurs in comparison if the magnitude of the two stimuli

are smaller than the average magnitude of entire set of stimuli presented because the subject overestimates the first stimulus, perceiving it as closer to the prior (expected) value of all stimuli. A similar argument with the drift of perception towards the prior can be made for the stimuli pair with the highest σ_1 value, which indeed gives rise to noticeable contraction bias in those stimuli as well.

It was already shown that when a rat learns the working memory task, it gives nearly equal weight to values of σ_1 and σ_2 to solve the task (Fassihi et al., 2014). We could replicate this behavioral analysis. To investigate if the rat strategy was consistent, we evaluated the weights that rat gives to σ_1 and σ_2 in each session. Animal's choice was fit using a logistic regression as a function of $\log\sigma_1$ and $\log\sigma_2$. The weights w_1 and w_2, namely their value and their ratios, tell us whether the rat uses both stimuli. We performed this analysis separately for each of the last 10 sessions of training before surgery and recording sessions. The results for one rat (ve15) are shown in Figure 3.3. This rat clearly used both stimuli to make its choice. Similar analysis for the three other rats was performed with the results illustrated in Figure A.1 to A. 3 in Appendix.

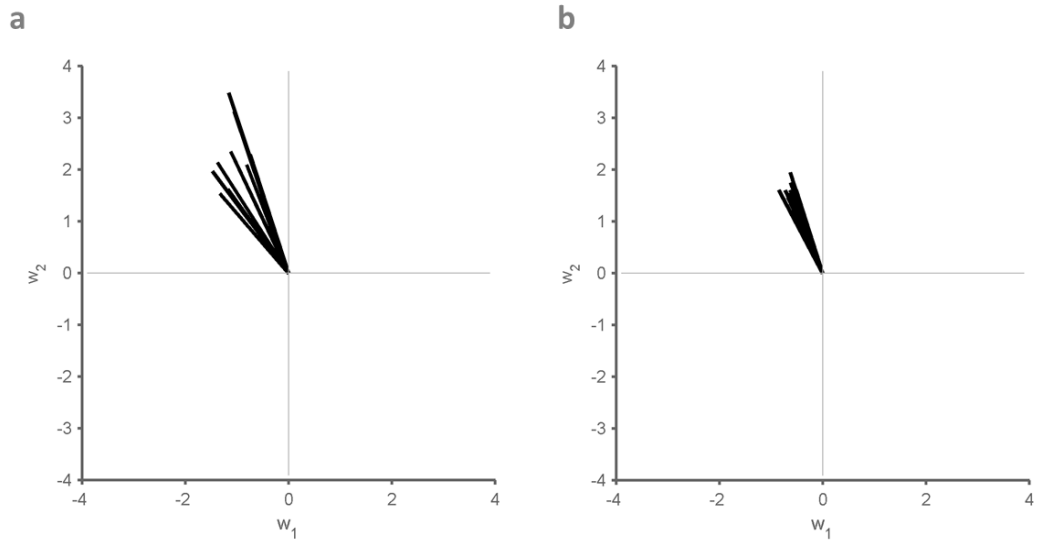

Figure 3.3. Weights of σ_1 and σ_2 in animal choice are represented by w_1 and w_2. Each (w_1, w_2) vector represents one session. Panel (a) shows last 10 training sessions before surgery while panel (b) illustrates the weights for the recording sessions of the same rat after surgery.

3.2 SII Recording in Anesthetized Rat

Neuronal responses to vibratory stimuli in cortical area SII were recorded in one rat under anesthesia. After the array penetrated the whisker SII cortex (see Methods chapter), vibratory stimuli were applied on the whiskers. Similar to the working memory task in behaving animal, the stimuli were delivered using a plate attached to a shaker. The plate was covered with a double-sided adhesive and the whiskers were attached to the adhesive. Stimuli with 7 varying σ values were delivered in random order with 50 repetitions per each stimulus.

In total 36 single units were isolated in the two sessions of recording. We calculated the Spearman correlation between the spike count during stimulus presentation and the σ value. In the neurons with significant correlation ($p<0.05$) the Spearman's rho was taken as an index for the strength of stimulus coding.

The spike count of 28 out of 36 neurons showed significant correlation with sigma value of the stimulus. The average rho coefficient of these neurons was 0.31 (ranging from 0.10 to 0.72 and standard deviation 0.15). Among the isolated neurons, none had significant negative correlation with sigma value. Spearman Rho for the set of recorded neurons is shown in Figure 3.4a. In Figure 3.4b the variation of the spike count of one SII neuron with high correlation for different stimuli is shown.

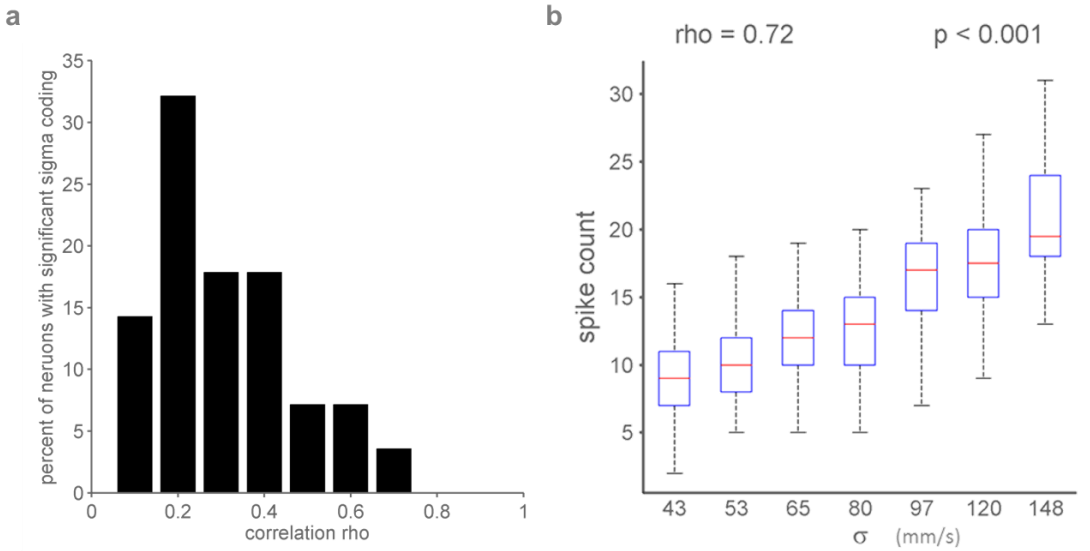

Figure 3.4. Coding of vibratory stimuli in SII neurons in anesthetized rat. (a) Distribution of correlation rho in neurons with significant coding. (b) Spike count of a SII neuron with high correlation with vibratory stimuli in anesthetized rat is depicted. The neuron produces more spikes in response to stimuli with greater σ value.

After studying SII response in the anesthetized rat, we proceeded to investigate the activity of neurons in SII region of behaving animals.

3.3 SII Recordings in Behaving Animal

One rat (ShT2) was trained to perform the tactile working memory task. After training, single units of whisker-related SII were recorded extracellularly as the rat performed the parametric tactile working memory task. We recorded from 36 single units in this rat in 2 sessions. The timeline of the trial shown in Figure 3.5.

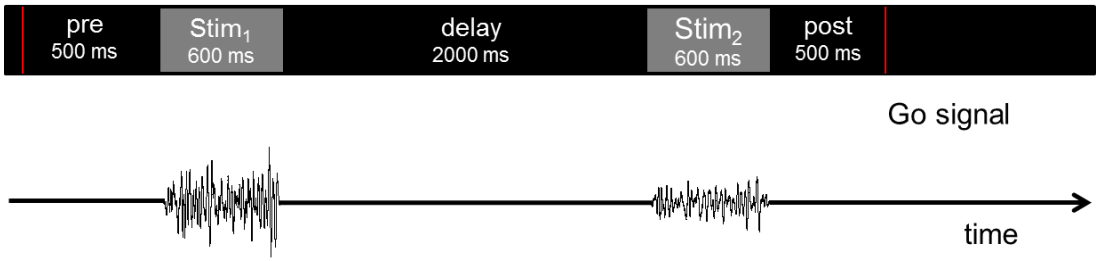

Figure 3.5. Timeline of trials. The animal received the first stimulus, maintained its memory during the delay, received the second stimulus and compared the two stimuli to make the two forced-choice action.

The data analysis was carried out only for trials with correct responses. We used two criteria for assigning different functions to the neurons. The first criterion considered Spearman correlation between the spike count and the task parameter at relevant epochs. In order to investigate the activity of each neuron, spikes were binned over 100-ms non-overlapping windows for each trial. The Spearman correlation between spike counts in each bin with the following parameters was tested:

- First stimulus value (σ_1)
- Second stimulus value (σ_2)
- Comparison rule (σ_2- σ_1), as an indication of the decision of the animal

Any neuron which was significantly correlated with σ_1 for at least 2 bins out of 6 during the first stimulus presentation was classified as a $Stim_1$ coder. Similarly, a neuron was classified as a $Stim_2$ coder if the correlation in 2 bins out of 6 was significant. According to our criterion, 8 neurons (22.2 %) were $Stim_1$ coders. One example is shown in Figure 3.6.

Out of 36, 8 (22.2 %) were classified as $Stim_2$ coders. Figure 3.7 illustrates the response of the same neuron of Figure 3.6 during $Stim_2$. Although there were overlaps between $Stim_1$- and $Stim_2$- coders (3 neurons), not all $Stim_1$ coders were necessarily $Stim_2$ coders.

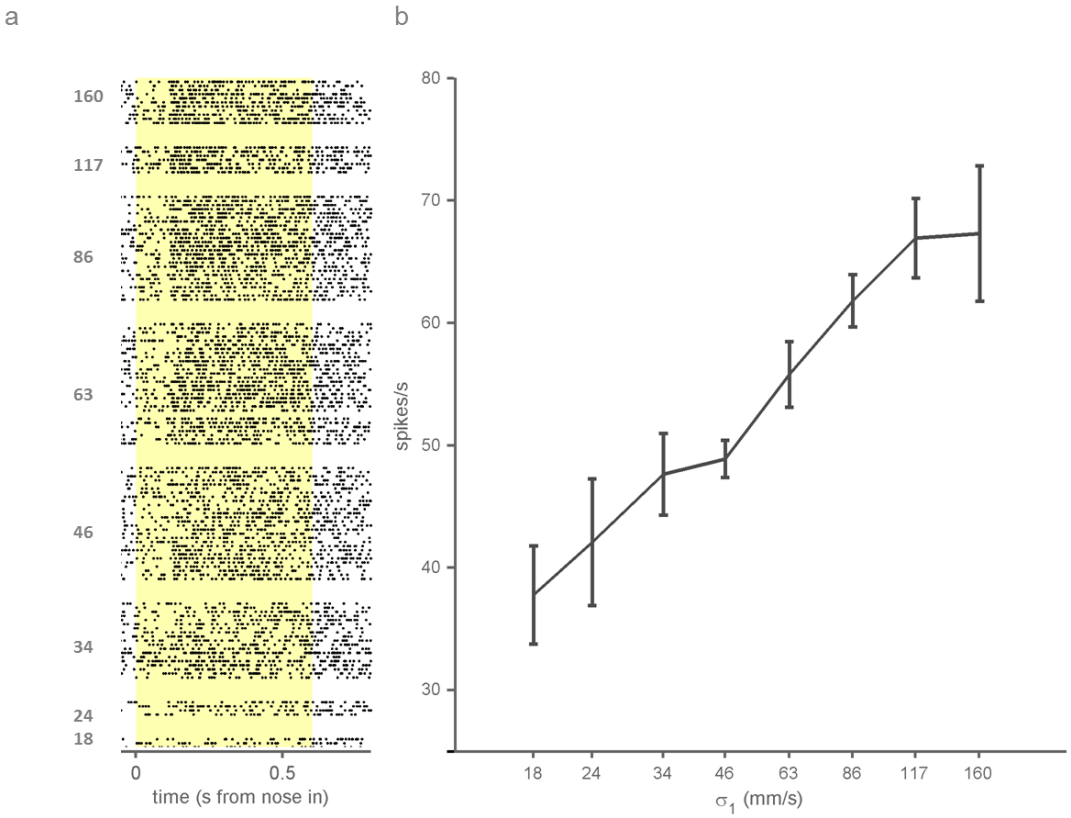

Figure 3.6. An SII neuron with a sigma-coding response to $Stim_1$. (a) Raster plot of response to $Stim_1$. Trials were delivered in random order but for visualization, the trials are grouped according to the σ values which are the labels on the left side. (b) Average firing rate during the last 400 ms of the $Stim_1$. Yellow shade is the stimulus presentation window. Errors bars, in this and subsequent figures, are standard errors.

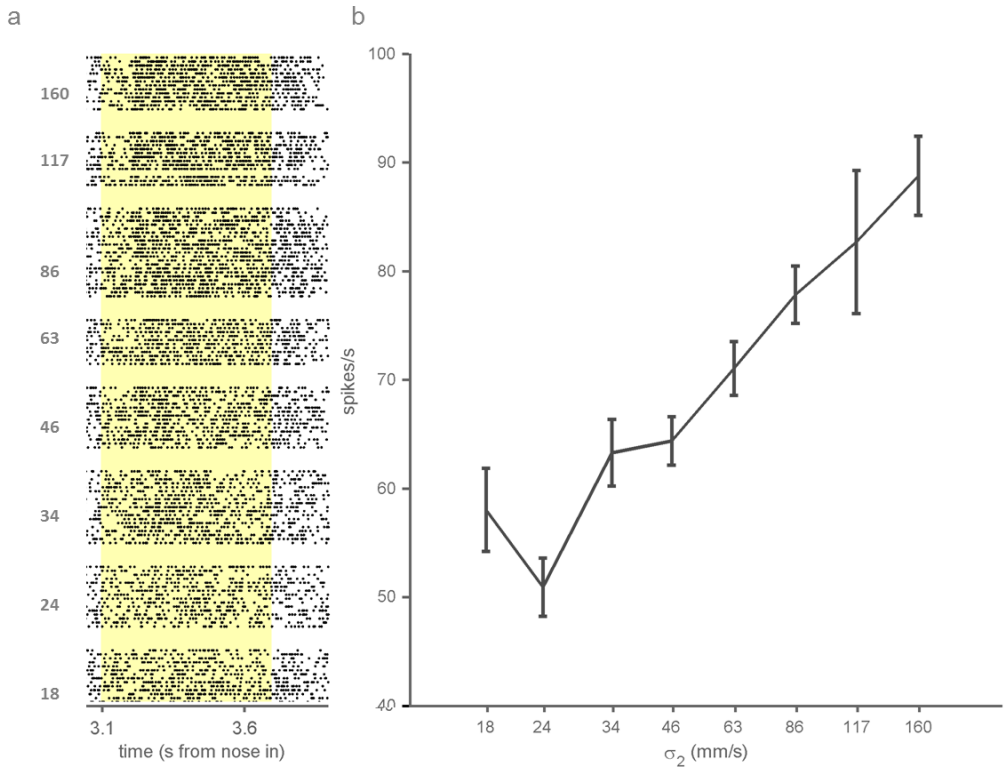

Figure 3.7. An SII neuron with a sigma-coding response to $Stim_2$. (a) Trials are grouped based on σ_2 value. (b) Average firing during the last 500 ms of the $Stim_2$.

8 neurons (22 %) were classified as decision-coding neurons, as they didn't respond in a purely sensory manner to σ_2. The firing of these neurons was correlated with the comparison rule (σ_2- σ_1), which means that the response to $Stim_2$ was not simply a function of σ_2.

For a more general analysis and as the second criterion to classify neurons, we considered the possibility of the dependence of response during $Stim_2$ could be a function of both σ_2 and σ_1. We chose a planar function of σ_2 and σ_1 and approximated the firing of neurons to it. The function was as follows:

spike count = w_1*log σ_1 + w_2* logσ_2 + c

The coefficients w_1 and w_2, are measures of dependence of firing counts on σ_1 and σ_2, assuming a linear relation. The firing rate of each neuron over each of the epochs of $Stim_1$, $Stim_2$ and post-stimulus delay was fit with this function. The resulting w_1 and w_2 coefficients for each neuron are plotted in Figure 3.8.

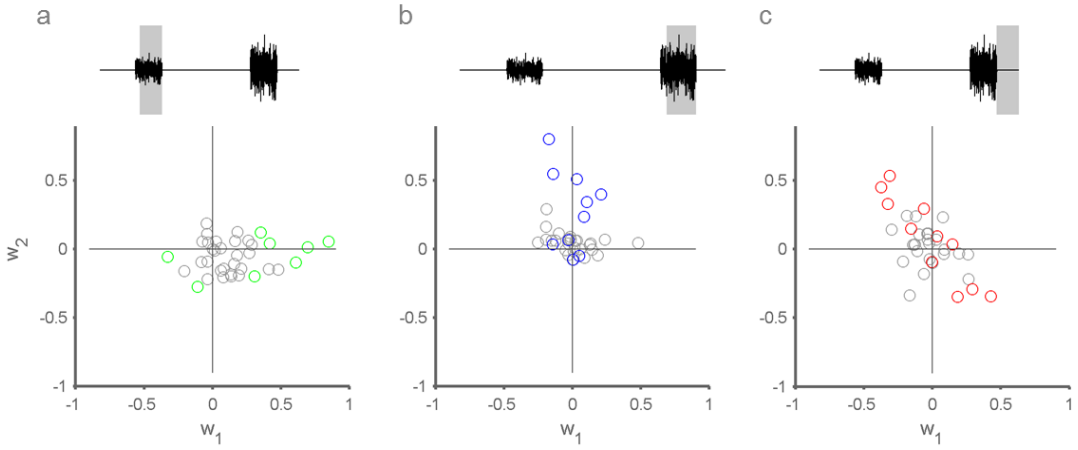

Figure 3.8. Set of single-neuron SII responses during 3 different epochs of the task represented as coefficients in a linear model. The gray shade above each panel indicates the time window over which the firing is fit for the corresponding panel. Each circle represents one neuron. (a) Responses during $Stim_1$. The population responses align to w_2 = 0 which indicated the dependence of neuronal firing on σ_1. Green circles are the $Stim_1$ coders that were classified by correlation analysis. Time window is from 600 to 1100 ms from nose-poke. (b) During $Stim_2$, the population deviates from w_2 = 0 and the $Stim_2$ coders that are shown in blue, become aligned to the w_1 = 0. The majority of neurons does not respond in a purely sensory manner to σ_2. Time window is from 3200 to 3700 ms from nose-poke. (c) Population response becomes aligned to w_1= - w_2 axis which can indicate the comparison that leads to the decision of the animal. Time window is from 3700 to 4200 ms from nose-poke.

Three lines are of particular interest in this figure: $w_1 = 0$ axis and $w_2 = 0$ axis and $w_1 = -w_2$. The points that fall on $w_2 = 0$ axis are responses that depended merely on σ_1 while the points lining on the $w_1 = 0$ were only dependent on σ_2. These two are purely sensory responses. The points that lie on $w_1 = -w_2$ represent responses that depended on the comparison rule of $\sigma_2 - \sigma_1$. The responses at the beginning are dependent on σ_1 and during the second stimulus it tends toward σ_2 and gradually become aligned to $w_1 = -w_2$ axis.

To investigate the behavior of the population during the delay period, the same analysis in windows of 500 ms of length was also performed and the results in the four windows of time during delay are shown in Figure 3.9. There is no clear alignment of the population around either axes or diagonal line of comparison.

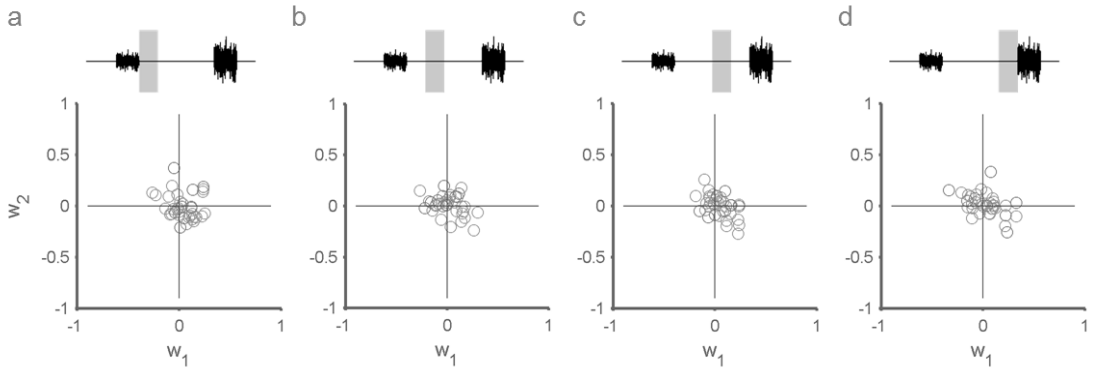

Figure 3.9. Set of single-neuron SII responses during delay of the task represented as coefficients in a linear model. Panels (a-d) illustrate the arrangement of neurons with respect to the axes and comparison diagonal line in 4 windows of time with the length of 500ms.

In order to investigate the change of the firing rate of each single neuron during the task, we approximated the firing of each neuron in sliding 200ms windows. The resulting coefficients for a representative SII neuron are shown in Figure 3.10. Each symbol in each panel corresponds to a planar fit, separated from its neighbors in steps of 25 ms. During Stim1, the planar fits line mainly on $w_2 = 0$ while it moves toward the central nonsignificant w_1 weights during the delay. By the start of second stimulus, the dynamic of response changes and w_2 grows, indicating dependence on σ_2. During the post-stimulus delay, when the animal has to make the decision and maintain it until the go signal, the neuronal firing falls around the $w_1 = -w_2$ line which is representative of comparison.

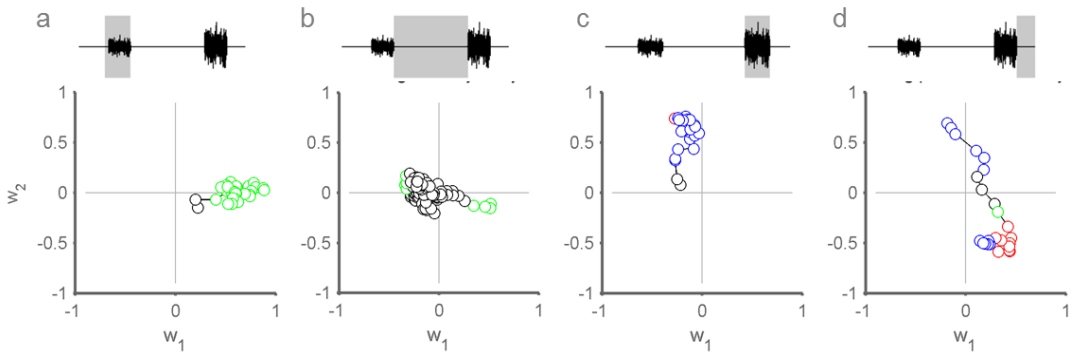

Figure 3.10. Response dynamic of one SII neuron during different task epochs. The gray box above each panel represents the epoch of the task that the firing counts over sliding windows of 200 ms are approximated with planar fit. Each symbol represents a planar fit that is separated from its neighbors by 25 ms. (a) Main determinant of neuronal response during first stimulus presentation was σ_1 and green symbols indicate the fits with w_1 significantly different from 0 ($p<0.01$). (b) Planar fits during delay lie around $w_1 = 0$ however the majority of the fits did not have w_1 significantly different from zero. (c) As the second stimulus was presented, neuronal response became dependent on σ_2, indicated by the larger w_2 in comparison with earlier epochs. Blue edges indicate fits with w_2 significantly different from 0 ($p<0.01$). (d) By the end of Stim2, the neuron's firing was aligned on $w_1 = -w_2$ which suggests that the comparison ($\sigma_2 - \sigma_1$) was taking place to lead to the correct decision as both first and second stimulus were taking into account. For fits where both w_1 and w_2 were significantly different from zero, the symbols are colored in red.

This dynamic during the course of trial from the beginning to the go signal of the same neuron is shown in Figure 3.11 show the gradual change of planar fit as the time of the trial evolves.

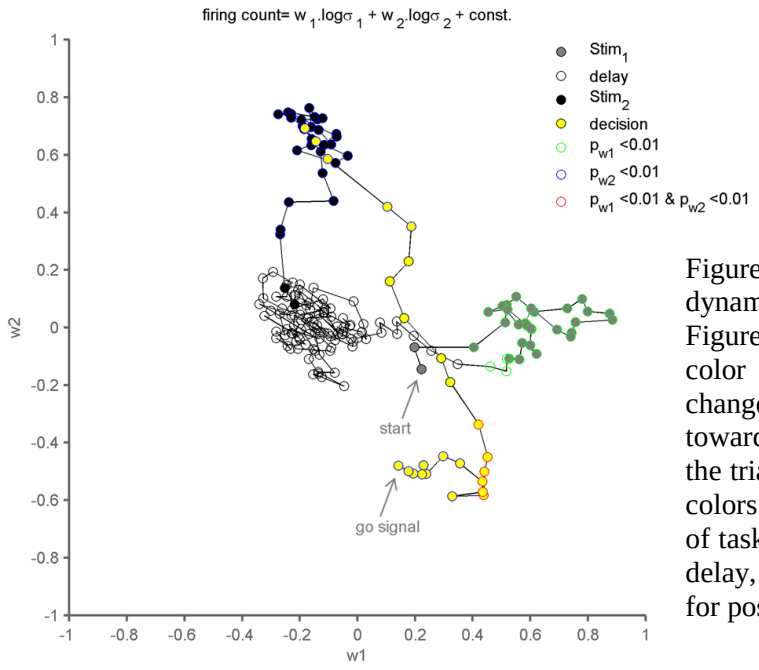

Figure 3.11. Change of response dynamics of the same neuron as Figure 3.9 over time The same color code is used. The gradual change of response dependence towards w1=-w2 line is clear as the trial timeline evolves. The face colors of circles indicate the epoch of task as grey for $Stim_1$, white for delay, black for $Stim_2$ and yellow for post stimulus delay.

Different dynamics were evident in different neurons. The dynamics of responses of three other exemplar neurons are depicted in Figure 3.12, 3.13 and 3.14.

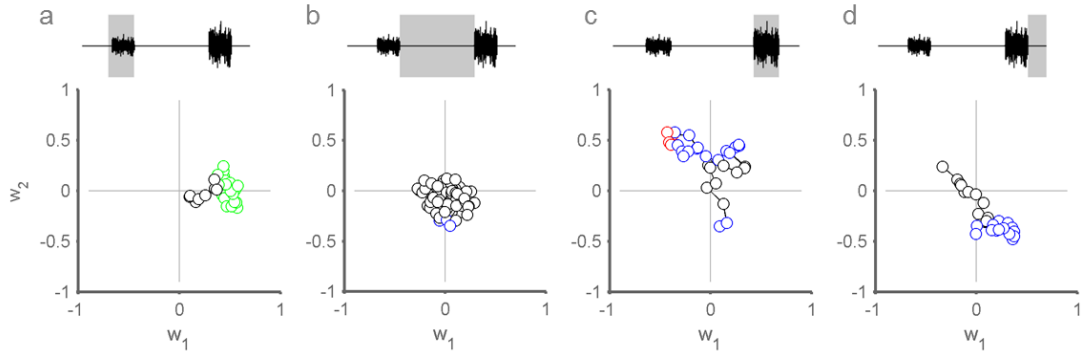

Figure 3.12. The response dynamics of a neuron coding comparison without sensory coding The panel explanations are the same as Figure 3.6. The neuron coded the decision during post stimulus delay. In this particular neuron, the dynamic during $Stim_2$ depended on σ2 but slowly deviated more toward the line w1=-w2 closer to decision epoch.

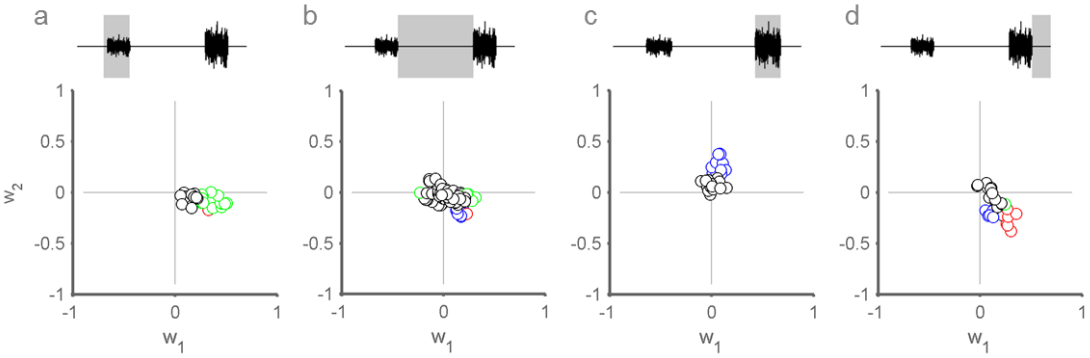

Figure 3.13. Another example SII neuron with sensory response to stimuli at the last 200 ms of the stimulus presentations. The firing during the post-stimulus delay was distributed along the comparison axis.

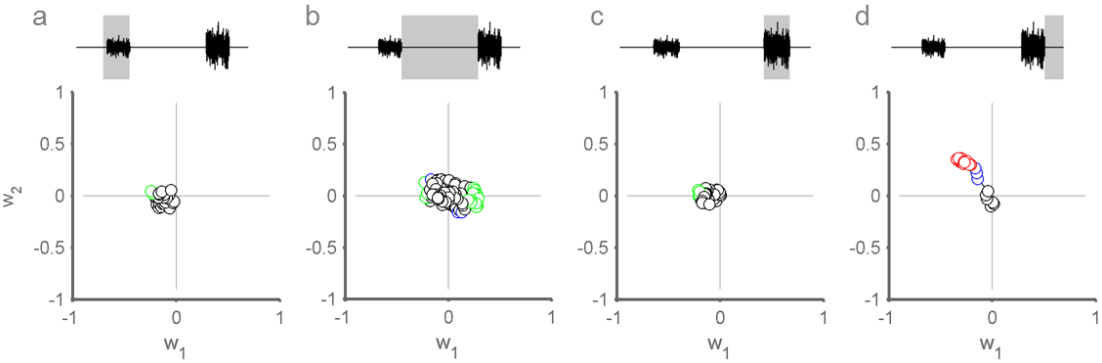

Figure 3.14. The dynamics of a neuron which did not respond in a sensory manner to either of the stimuli but showed comparison dependent activity during the decision period as the response aligned to $w_1 = -w_2$.

In order to estimate the proportion of neurons with dynamics proportional to $\sigma_2 - \sigma_1$, the firing of neurons from the start of $Stim_2$, was approximated with the following function:

Spike count = w_{choice} *(σ_2- σ_1) + constant

The bin window was 200 ms long that shifted in steps of 25 ms. In Figure 3.14, the proportion of population of SII neurons with w_{choice} significantly different from 0 is shown as the sliding window moved during the second stimulus and decision epoch. As $Stim_2$ started the proportion rose up to 0.15 in the middle of $Stim_2$ and this proportion peaked above 0.2 during the post-stimulus delay. To compute the chance level of the results, for each neuron, we shuffled the stimuli for 1000 times and ran the planar fit analysis. In the Figure 3.15, the chance level of significant w_{choice} averaged over all neurons, is shown in black trace centered at about 0.05 (as expected).

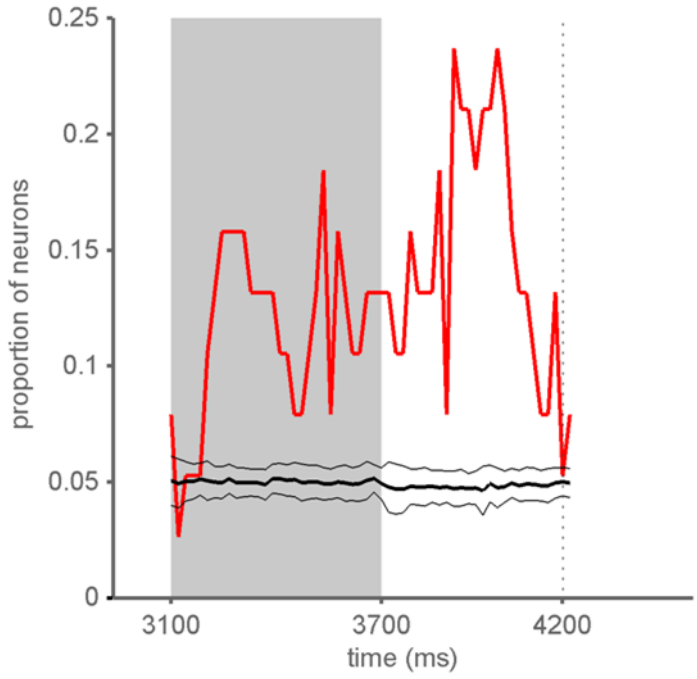

Figure 3.15. Comparison-based behavior of the population from Stim2 presentation to the end of trial (go signal). The proportion of neurons with w_{choice} significantly different from zero ($p<0.05$) as function of time is plotted in red. The black trace is significant weights for planar fit stimuli shuffled 1000 times and averaged over all neurons. The thin black lines indicated standard deviation of the shuffles.

In summary, a high percentage of SII neurons in the behaving animal during the WM task showed sensory stimulus coding during its presentation. In a substantial set of SII neurons, late in the presentation of the second stimulus and during the following delay before animal action, the neuronal activity became correlated with comparison rule, indicating a history dependent activity at this epoch.

3.4 Hippocampal Recordings in Behaving Animal

Three rats were trained in the tactile working memory task and then implanted in the left hippocampus. We recorded 20 sessions of neuronal data as these rats performed the working memory task.

One of the characteristics of hippocampus is the presence of theta oscillations, which is in the range of 6-10 Hz in rodents. In rodents, hippocampal theta has been found during active movements such as running, jumping, exploratory sniffing and whisking. We started our analysis of the hippocampal neuronal data by examining the presence of theta rhythms. As mentioned in the methods chapter, for each channel the power spectrum was calculated in the range of 1-300 Hz. Figure 3.16 illustrates the average power as a function of frequency. A prominent bump is evident in the range of theta oscillations (6-10 Hz).

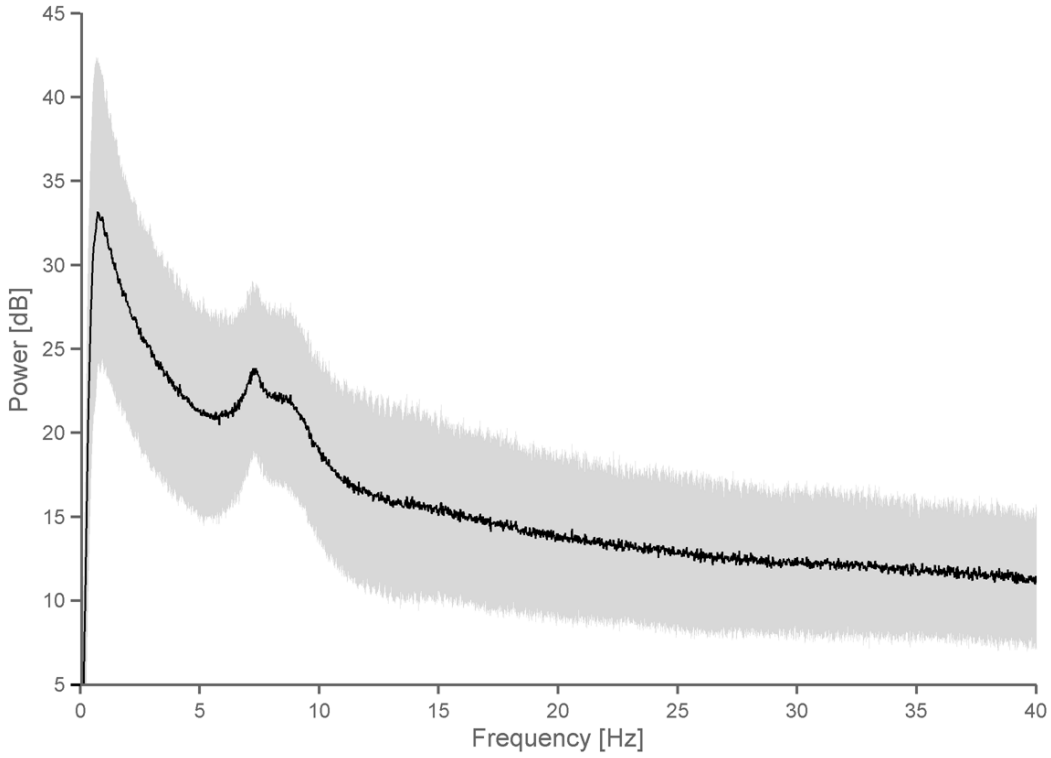

Figure 3.16. Average spectrum of channels across 10 sessions of one rat. The high power oscillation in the range of theta is clear. The grey shadow indicates mean +/-1 standard deviation.

Temporal modulation of the theta oscillations is shown in Figure 3.17. The analysis was performed on all trials and as mentioned in Methods, a window of 0.6 s with steps of 0.05 s was used for multitaper analysis. The average power within the range of 6-10 Hz is plotted as a function of time. The main changes in theta happened as the rat entered and left the nose-poke at the start and end of trials, however there is also a gradual increase in the power during trial.

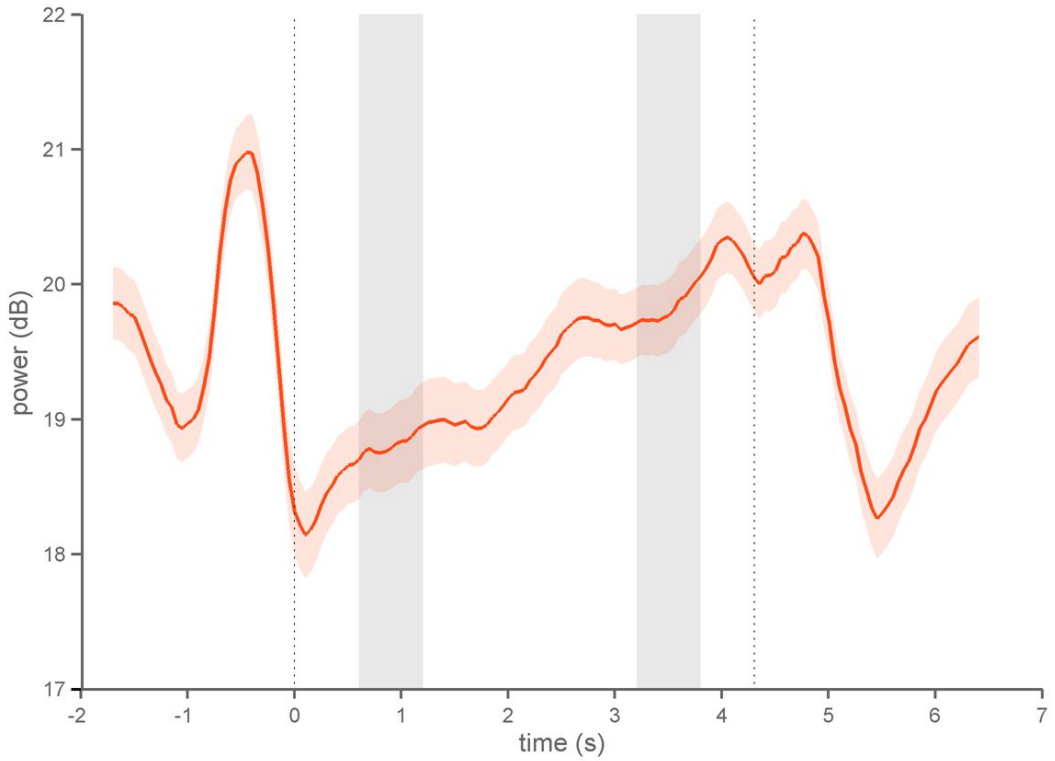

Figure 3.17. The temporal modulation of theta oscillations. Red solid line is the power averaged over the range of 6-10 Hz. Pink shading indicates the standard error of mean of the power. Gray shadings are the stimulus presentation times and left and right dashed lines represent entry into nose poke and 'go' cue, respectively.

Having confirmed the presence of characteristic theta oscillations in our recording from hippocampus, we moved to the analysis of the spiking activity of single units during the task. In total 214 single units were isolated from 20 sessions.

As the presence of place cells is well studied in hippocampus in other behaviors, we first checked for neurons with this property during our task. For simplification, we examined the cells that significantly coded the rats' choice of action. At the end of each trial, the animal needed to make a choice in turning either to the right or to the left reward spout. Therefore, the presence of the rat in the right or left reward spout

could be tracked through its decision after the go-signal. In this setting, we could only identify the place cells with place fields located by the proximity of the two reward spouts. We calculated the correlation between the rat's action and the spike count in the window of 1000 ms following the go cue. The mean reaction time of the animals was about 480 ms, therefore we are confident that the animal had chosen one of the two reward sites within this time interval. The correctness of the animal's action was not considered relevant for this part of analysis and so all trials were included.

Cells with a spike count significantly correlated with animal action are classified as place-coders, giving a count of 116 neurons (54%). 68 units had higher spike count for the right side/action and 48 for the left. Figures 3.18 to 3.19 illustrate examples of place-coding hippocampal neurons. We noted different patterns of activity for these neurons. Only for visualization purpose in Figures 3.18-3.20, a kernel with the length of 200 and sigma of 50 is used for smoothing in peri-stimulus time histogram. However, for none of the analysis, smoothing is applied.

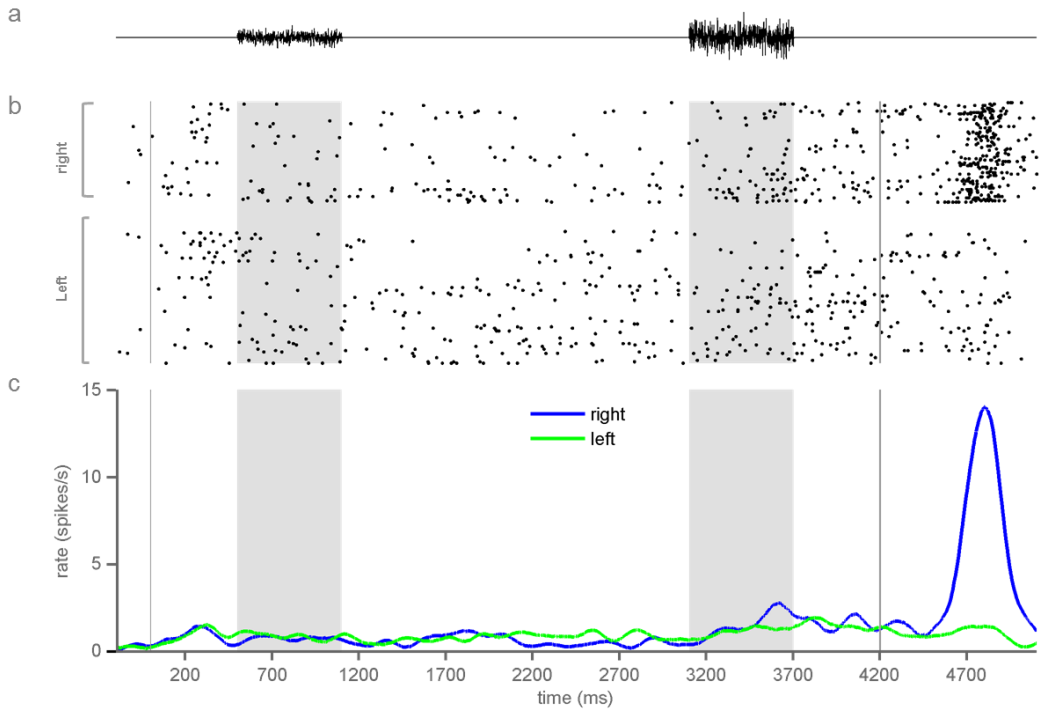

Figure 3.18. A neuron with elevated firing for the right reward spout. Panel (a) shows an example of the stimuli over time. Panel (b) illustrates the raster plot of the neuron. The trials are sorted in two bands according to animal action. In panel (c) the blue and green trace respectively show the PSTH on trials that rat turned to right and left. This neuron became active in each trial that the rat turned to right irrespective of correctness. Shaded areas show the time of presentation of Stim1 and Stim2.

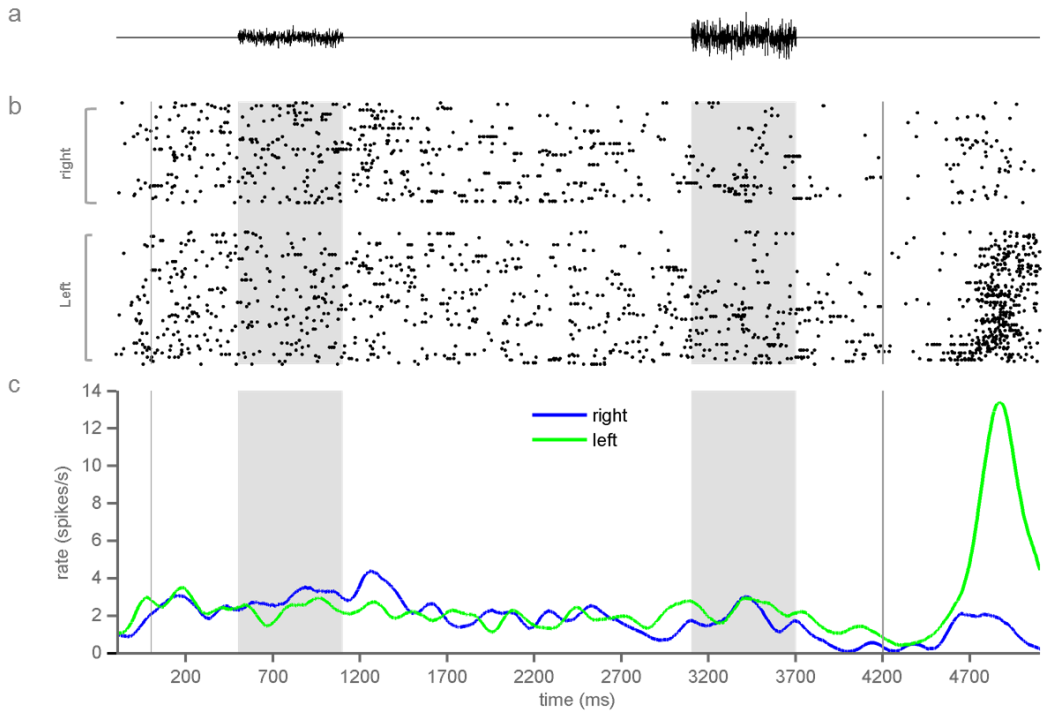

Figure 3.19. A unit that was selectively active for left reward spout. The order and description of panels are similar to Figure 3.17.

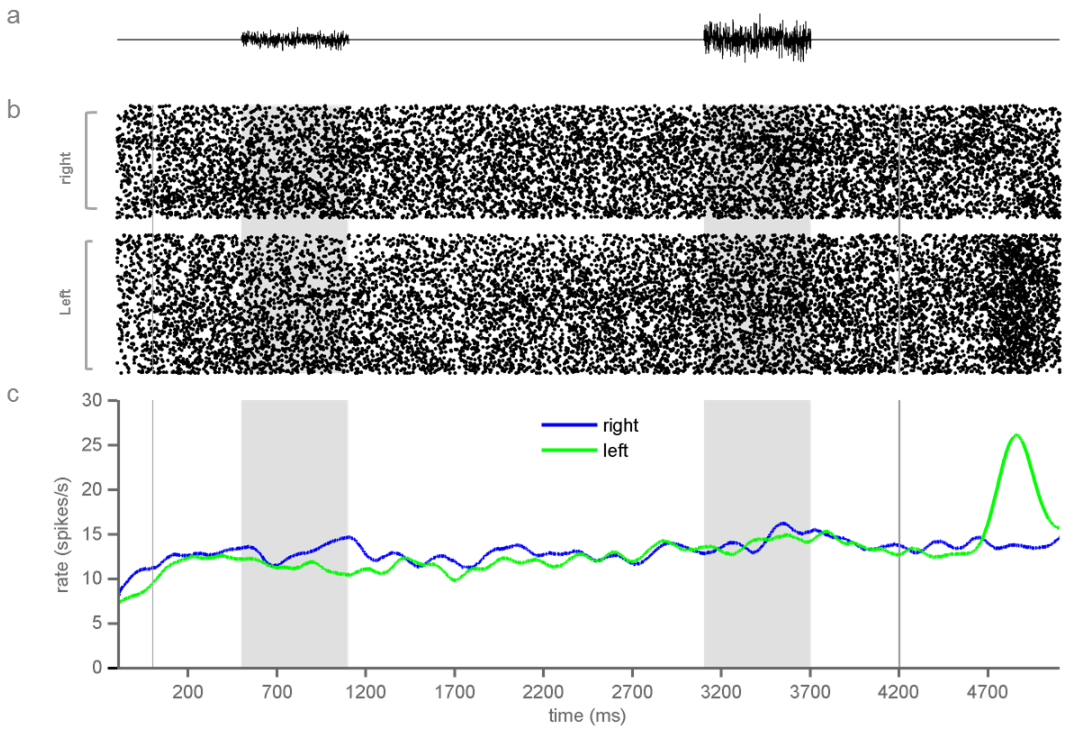

Figure 3.20. A unit with high baseline activity during trial with a surge in firing rate for left reward spout.

Place coding neurons had two distinct firing patterns during the trial timeline. Some like those illustrated in Figures 3.17 and 3.18 had low firing rate until the rat took the action (potentially pyramidal neurons). Another type of place coding neuron had baseline activity mainly in the range of 10- to 30 spikes/s and continued to fire at this rate as the rat occupied the "non-preferred" side. However the activity significantly increased in the suspected place field. One example is shown in Figure 3.20.

A second group of neurons were classified as ramping neurons; the firing rates of this group varied systematically with time during the task; more specifically the firing rate of these neurons changed markedly as the delay period unfolded. We identified 33 neurons with firing rate modulated along the trial timeline. Both upward and downward activity was observed in different sets of neurons. Two samples of such neurons are shown in Figures 3.21 and 3.22.

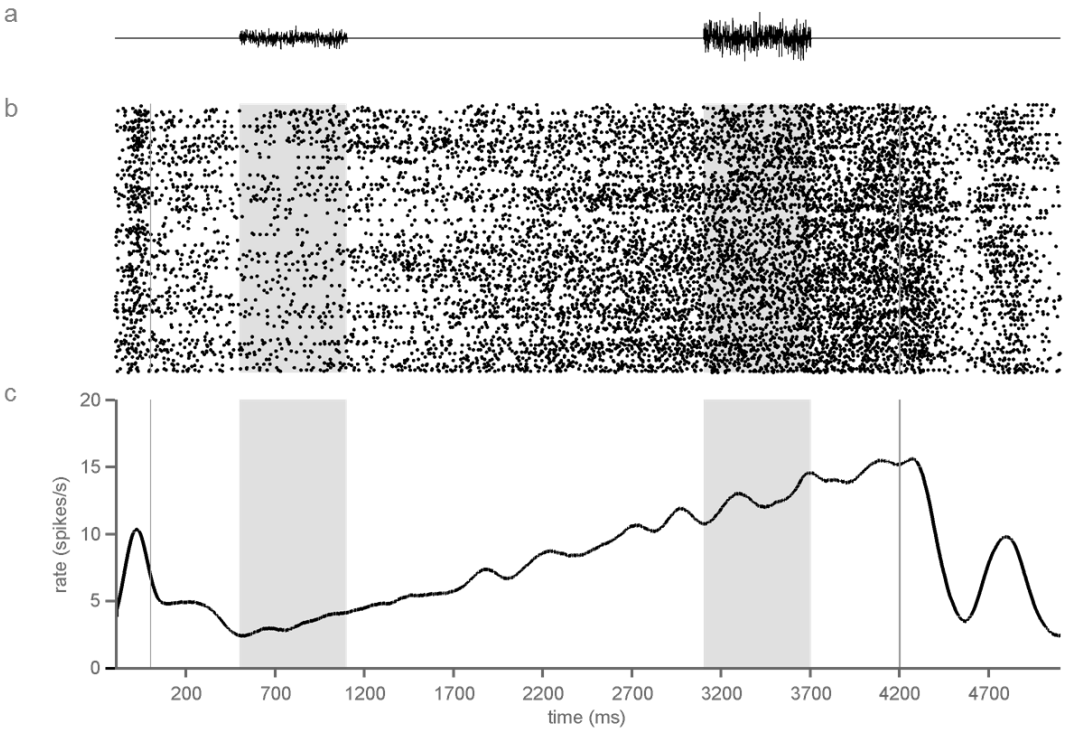

Figure 3.21. A ramping neuron with an increase in firing during trial that is followed by a drop in firing rate

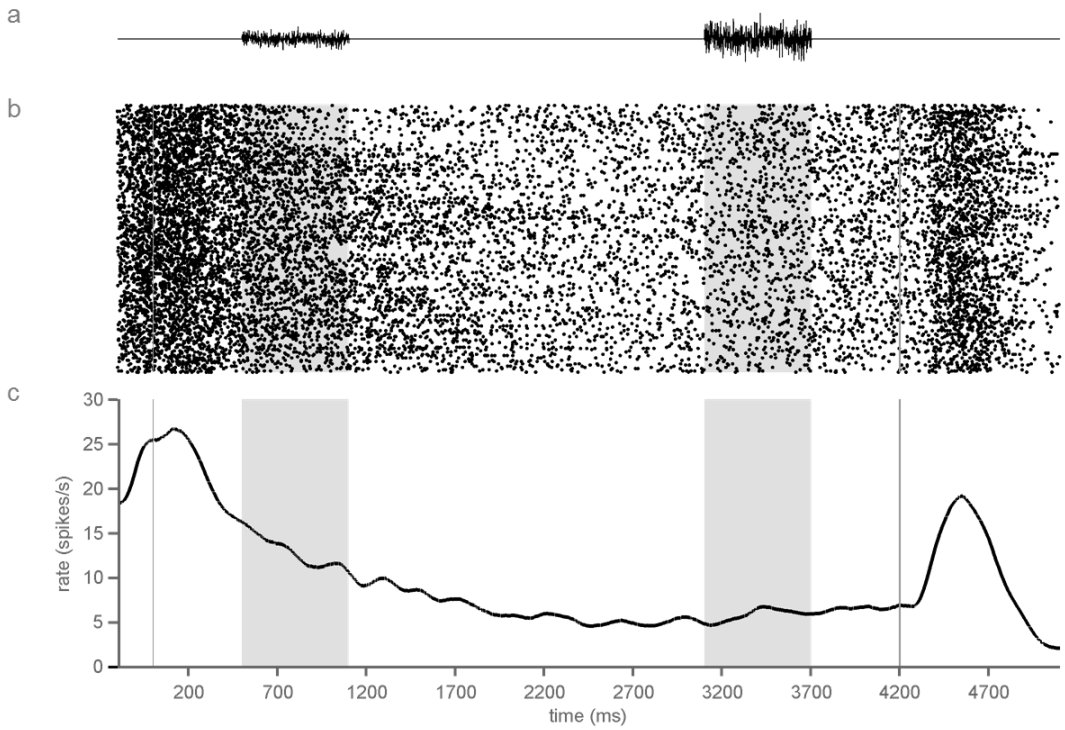

Figure 3.22. A down-ramping neuron. This neuron had a decrease in firing rate during trial, followed by an increase at the decision time.

To classify neurons functions according to task parameters, we performed a correlation analysis across time in non-overlapping bins, similar to that performed on SII neurons. Any neuron which was significantly correlated with σ_1 in at least 2 bins out of 6 during the first stimulus presentation was classified as $stim_1$-coder. Likewise neurons with significant correlation with σ_2 in at least 2 bins out of 6 of $Stim_2$ were considered $stim_2$-coders. In 3 rats in which we recorded from left hippocampus, in total 11 neurons (5.1%) were classified as coding $Stim_1$ during its presentation. 12 out of 214 (5.6%) were classified as coding $Stim_2$ according. One example of a neuron coding $Stim_2$ is shown in Figure 3.23. During presentation of the $Stim_2$, the neuronal firing decreased monotonically with increasing value of σ_2.

None of the neurons were classified as coding both $Stim_1$ and $Stim_2$, suggesting that we did not sample any hippocampal neurons with purely sensory properties. It should be noted that by the significance threshold of $p<0.05$, the number of neurons found to encode the stimulus was hardly greater than chance (5.1% for $Stim_1$ and 5.6% for $Stim_2$). Therefore the most conservative and safest interpretation of the data is that the analyzed set of hippocampal neurons did not encode σ value, at least not by the simple measure of firing rate.

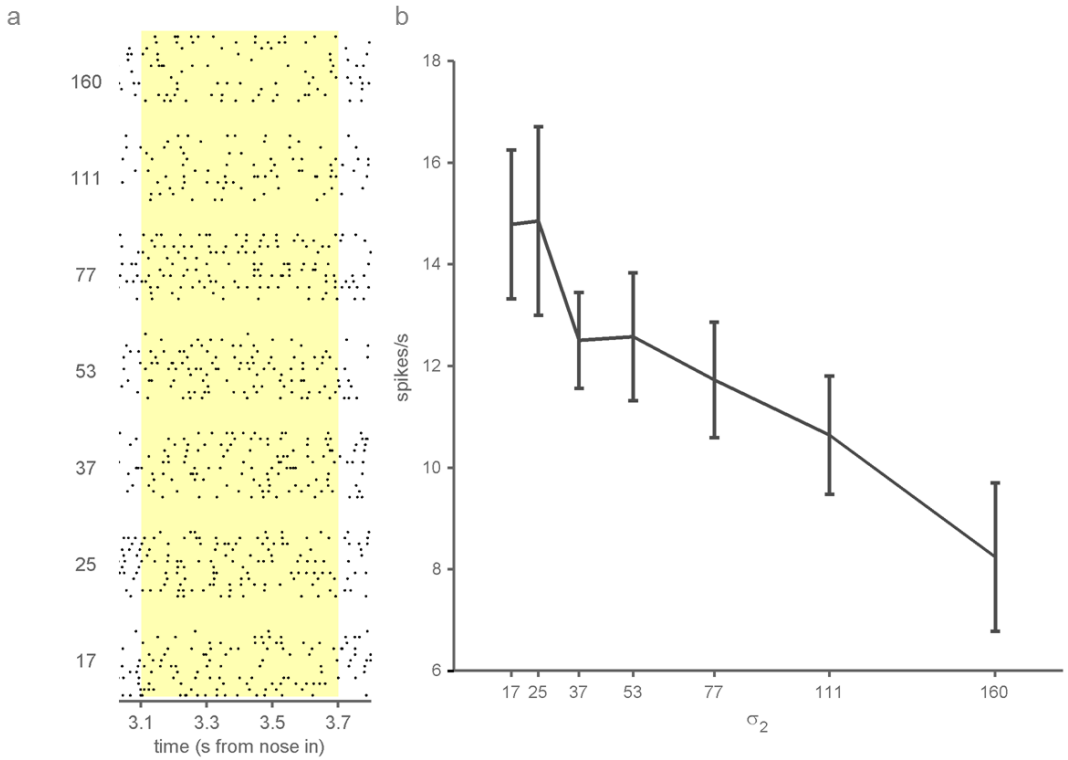

Figure 3.23. Firing of a neuron that encoded σ of $Stim_2$ during stimulus presentation. (a) The yellow shading highlights the $Stim_2$ presentation time. The trials are grouped according to σ_2, shown beside each group. (b) Average spike count during stimulus presentation. Error bars are standard errors.

If a neuron's activity showed a significant correlation with the comparison rule in at least 2 bins of post stimulus delay, it was assigned to the decision-coding group. 12 neurons (5.6%) coded the decision of the animal during the post-stimulus delay. A decision-coding neuron is shown in Figure 3.24. The trials are divided into two groups based on the comparison rule ($\sigma_1 < \sigma_2$ and $\sigma_1 > \sigma_2$). This neuron encoded the σ value of $Stim_2$ during its presentation and the two curves for the two actions overlap closely as the response depended mainly on σ_2. However, by the end of $Stim_2$, the firing of the neuron was modulated by the upcoming action of the animal. During this period the firing of the neuron depended not only on $Stim_2$, but also began to separate into two levels of firing rate according to the category (left or right) that the stimulus pair belonged to.

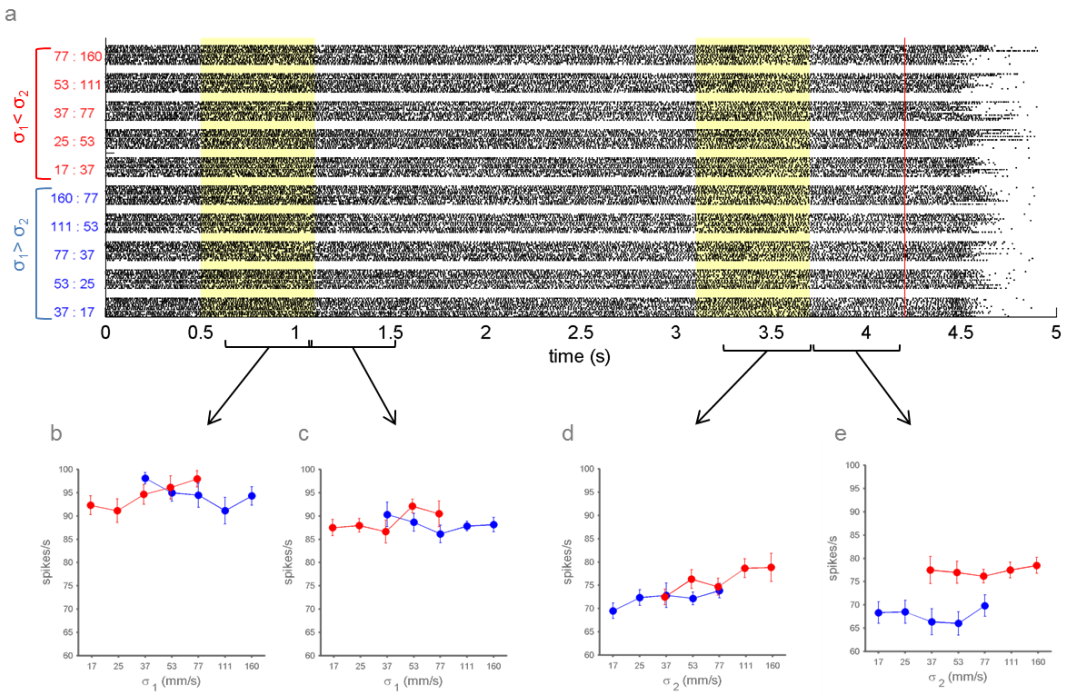

Figure 3.24. Putative hippocampal decision neuron. (a) Raster plot of firing along the task timeline. The trials are grouped by stimulus pair with labels for each group on the left side of vertical axis (σ_1: σ_2) (b) Average firing rate during the final 500 ms of $Stim_1$. Red and blue traces indicate firing rates for trials with $\sigma_1 < \sigma_2$ and $\sigma_1 > \sigma_2$, respectively. There was no monotonic coding of first stimulus in this neuron during $Stim_1$. (c) Average firing during the first 500 ms of the delay period. (d) The average firing during the last 500 ms of the $Stim_2$ carried information about σ_2. The two groups of trials that belong to two different possible actions, did not differ at this period. (e) During the post stimulus delay, as the rat awaited the go cue, there was no direct information about $Stim_1$ or $Stim_2$ alone, as both of the lines are almost horizontal. Firing rate separated according to future action.

To further examine this choice-correlated activity, we analyzed the error trials for these neurons. Spearman correlation between the spike count during post-stimulus delay with the animal action was calculated. In 9 out of 12 decision coding neurons, there was no significant correlation between action and firing of neuron. This is suggestive that the observed choice correlated activity of decision coding neurons on correct trials during the post-stimulus delay depended on stimulus perception and it was not merely a prediction of animal action independent of task parameters.

To investigate the overall change of the neuronal population in different epochs of the task, the firing of each neuron was approximated as a function of σ_1 and σ_2 in each epoch of the task with the function:

spike count = $w_1 * \log \sigma_1 + w_2 * \log \sigma_2 + c$

Similar to the analysis of the SII neurons, we inspected the distribution of neurons in a plane of w_1 and w_2 in the population of hippocampal neurons in Figure 3.25. Unlike the SII population, where we saw sensory response in most of the neurons, in the hippocampus we observed sensory response in less than 5% of the neurons. The decision neurons were distributed along the $w_1 = -w_2$ diagonal during the decision epoch (post stimulus delay).

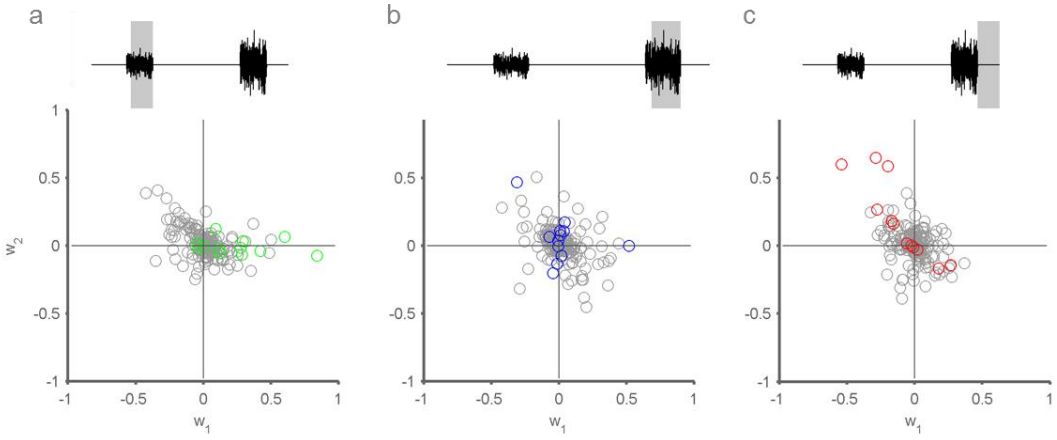

Figure 3.25. Hippocampal population response in different epochs of the task. The weights refer to window of $Stim_1$ from 600 to 1100 ms.in (a), window of $Stim_2$ from 3200 to 3700 in (b) and window of post-stimulus delay from 3700 to 4200 ms in (c) from the nosepoke.

Firing of neurons during the delay period was also fit with the above-mentioned function in four non-overlapping windows of 500 ms. The results are shown in Figure 3.26. During the delay, there is no apparent alignment of population along $w_2 = 0$; therefore, no memory coding in the population is observed.

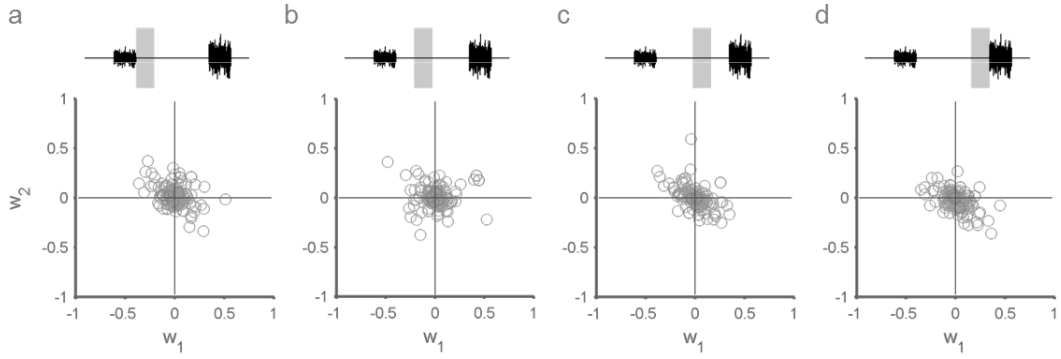

Figure 3.26. Hippocampal population response during delay. Weights in 4 non-overlapping windows of 500 ms are shown in (a-d).

In the next step, in order to study how the neuronal population dependence on comparison rule (σ_2- σ_1) changed during the $Stim_2$ and decision delay, the firing of each neuron was fit as a function of the choice:

Spike count= w_{choice} *(σ_2- σ_1) + constant

in bins of 200 ms that were shifted by 25 ms. It is important to emphasize that this time period is different from the action period during which the place coding properties of neurons were evident. Side coders were identified as the animal made the decision after the go signal and committed an action; by contrast, in this section, our analysis focuses on the activity of the neurons prior to the nose poke withdrawal and does not contain the action component of the animal behavior. The proportion of neurons with w_{choice} significantly different from 0 is plotted as a function of time in Figure 3.27.

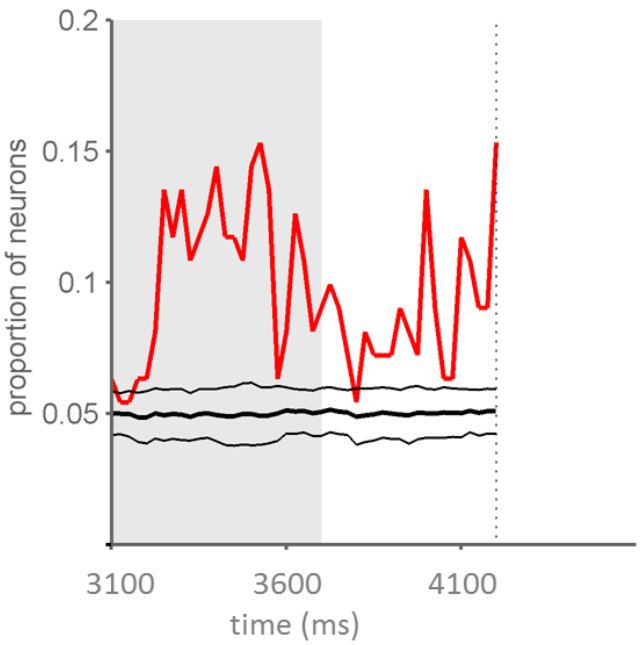

Figure 3.27. Comparison-based behavior of the population from Stim2 presentation to the end of trial (go signal). Gray shading represents Stim2 presentation time. The proportion of neurons with w_{choice} significantly different from 0 ($p<0.05$) as a function of time is plotted in red. The black trace is significant weights for planar fit for 1,000 times shuffled stimuli averaged over all neurons. The thin black lines indicate standard deviation of the shuffles.

Finally, to compare the activity of SII and hippocampus, the change of firing dependence on Stim1 and Stim2 are plotted in Figure 3.28 for SII (panel a-b) and hippocampus (panel c-d) ,respectively. Spike count within bins of 200ms was approximated as a function of σ_1 until the end of delay. During the first stimulus, there is a significant degree of sensory coding in SII population but in hippocampus this coding is at chance level. In SII, the trace of the sensory stimulus remains in the early phase of the delay; in about 15% of SII neurons the firing depends significantly

on sigma σ_1 during this epoch (see Figure 3.28) but there is no such prominent sustained activity in hippocampus. As $Stim_2$ starts, the firing of the neurons can be approximated as a function of $Stim_1$ (memory) and the ongoing $Stim_2$. During $Stim_2$ presentation, the stimulus coding is prevalent among SII neurons. Stimulus coding during $Stim_2$ is observed among hippocampal neurons with much lower frequency, near the expected chance frequency of 5%.

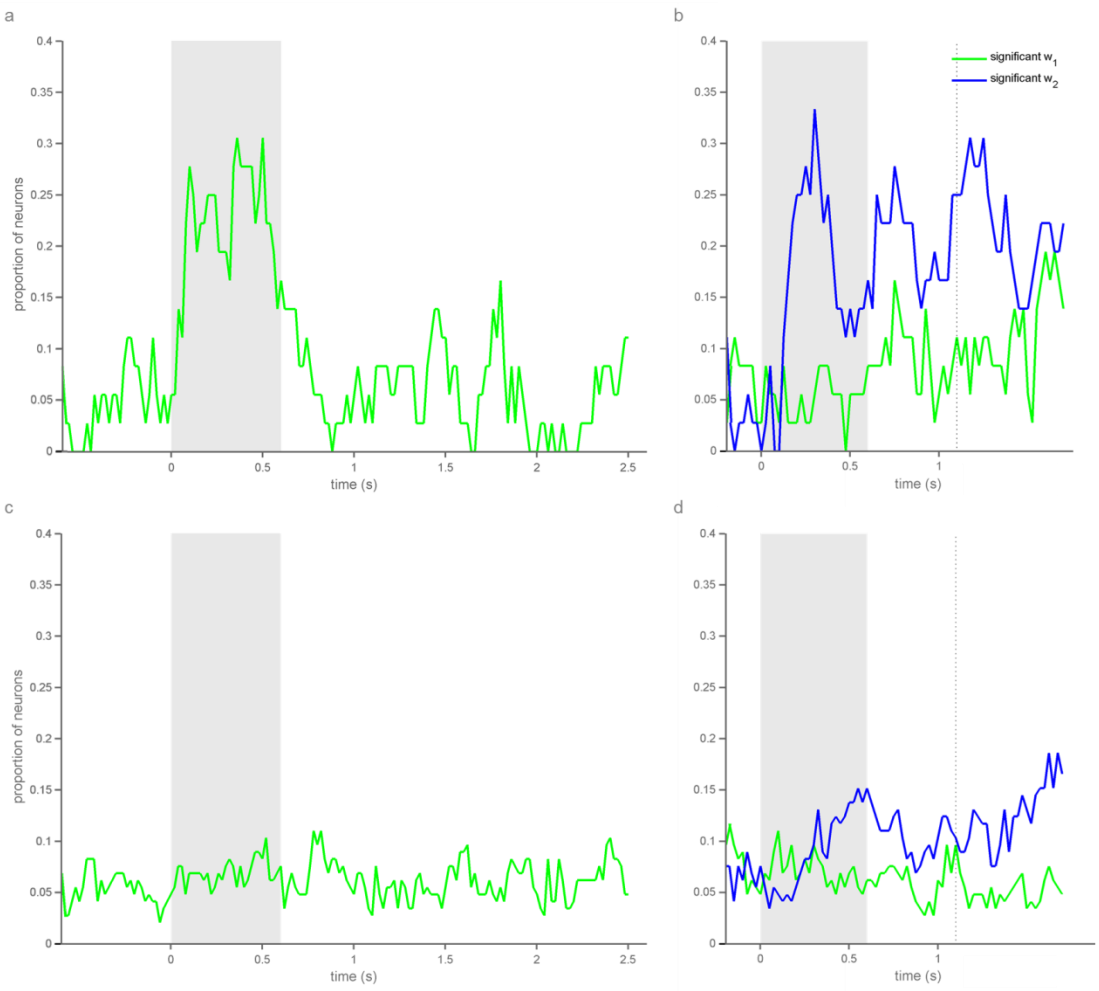

Figure 3.28. Change of proportion of neurons with stimulus-dependent firing in SII and hippocampus (a) The firing of each neuron of SII is approximated as a function of σ1 (firing count= w_1* σ_1+c) in shifting windows that moved in steps of 25 ms until the end of delay. Green trace indicated the proportion of neurons whose activity were modulated by significant weight for σ_1. Gray shade represents the stimulus presentation time and dotted line is the start of trial by nose-poke (b) from the start of the second stimulus, the firing count was approximated as a function of both σ1 and σ_2 (firing count= w_1 σ_1+w_2 σ_2+c). The blue trace is the proportion with significant weight for σ2 while the green trace shows the proportion for significant w1. Gray shade is the stimulus presentation time. (c) Firing of hippocampal neurons is approximated as a function of σ_1 and the proportion of neurons with significant weight is shown in green trace. (d) Similar to panel (b) the firing of neurons in hippocampus is approximated as a function of both stimuli and the proportion of neurons with significant w_1 and w_2 are shown in green and blue traces.

In summary, in rats performing the tactile WM task, a high percentage of SII neurons in our sample showed sensory coding of the stimulus during its presentation. This activity shifted towards the comparison rule late in the presentation of the second stimulus and during the post-stimulus delay, indicating that both $Stim_1$ and $Stim_2$ affected the neuronal firing at this epoch. In particular, the spiking activity of many neurons in the SII population tilted towards $w_1 = - w_2$ which can be considered as a history-dependent response.

In the hippocampus of rats, place coding was prevalent among the neurons, as expected by the cognitive map theory. Task variables might be processed in hippocampus under other conditions, for instance if we were to change the reward rule unexpectedly. In contrast to SII, in the hippocampal population sensory coding was not observed beyond the chance level. However in the hippocampus, we identified neurons whose activity was choice-correlated during the post-stimulus delay and therefore both the σ_1 and σ_2 were factors affecting neuronal response. When firing of neurons are fit as a function of σ_1 and σ_2, all of these decision neurons as shown in red circles in Figure 3.26c aligned to the $w_1 = -w_2$ diagonal line. Although the proportion of these neurons in the set of our sample is low (about 5%), but the coding of decision is robust. Moreover, the choice correlated activity was not present in majority of decision neurons in error trials suggesting that decision correlated activity was dependent on the correct perception of the stimuli and was not merely a reflection of future action of animal.

4 Discussion

A wide variety of cognitive abilities are dependent on a functional working memory system. In the setting of tactile working memory task, two noisy vibratory stimuli, separated by a delay, were applied on rats' whiskers and rats had to compare the σ of $Stim_1$ and $Stim_2$ to make a two-forced choice decision. More precisely, in order to solve the task, the rats needed to perceive σ_1, keep its trace in memory during delay, perceive σ_2, compare σ_2 to the trace of σ_1 and choose an action based on this comparison.

Through multi-electrode recordings, we separately explored the activity of two brain areas in rats, SII and hippocampus, to unravel their engagement across different epochs of the parametric working memory task. We were particularly interested in the neuronal response dynamics that were relevant to the encoding of the physical stimulus, its maintenance during the delay and the comparison that could lead to the desired decision making.

SII lies lateral and anterior to SI and receives direct input of whisker system form ventral posterolateral thalamic nucleus (Pierret et al., 2000). Projections to and from a brain region are important in the models of functional connectivity of the cortex as they provide the basis for theories of hierarchical processing (Diamond et al., 2008). Connectivity studies in rats have confirmed that SI and SII are reciprocally connected (Alloway and Burton, 1985; Krubitzer and Kaas, 1990; Schwark et al., 1992; Catania and Kaas, 2001; Disbrow et al., 2003; Zakiewicz et al., 2014), while SII in turn projects directly to the primary motor cortex (Reep et al., 1990, Smith and Alloway, 2013) and through association areas, such as the perirhinal cortex, to PFC (Bedwell et

al., 2014). This pattern of connectivity to primary sensory and motor cortices and higher processing areas is suggestive of SII being a part of the core network that transits crucial whisker related information for animal behavior.

The major findings in our sample of SII neurons in a rat that performed the tactile WM task were as follows: (1) sensory coding of σ was prevalent among the sample SII population, and (2) choice related activity that depended both on σ1 and σ2 was also widespread late in the presentation of the second stimulus and during the post-stimulus delay. σ coding was prevalent in about 30% of our sample SII population, which is less than the σ coding of the SI population (Esmaeili, 2014). In SI, up to 60 % of neurons were engaged in σ coding during its presentation. Moreover, the trace of the σ_1 remains in the firing rate of neurons in SI and SII only during the early epoch of the delay, indicating that neither SI nor SII maintain the information about σ_1 during the entire delay. The percentage of the neurons keeping the σ trace in early delay in the SI was higher than that of SII (30 % compared to 15%).

The second finding, comparison related activity in about 25 % of the SII population is suggestive of the comparison taking place in SII. This comparison occurs late in the presentation of the second stimulus and during the post-stimulus delay and is correlated with this choice. Another evidence of choice related activity in SII was provided in rats' discriminating textures (Safaai et al., 2014). It is important to note that our results of SII lies in agreement with the results of SII recording in flutter discrimination task in monkeys, as neuronal correlates of decision making were also found in the fingertip region of SII (Romo et al., 2002). In their task, the rule to solve the task depended on the difference between the frequencies of the two stimuli (f2-f1), and the population activity reflected by the end of second stimulus tended towards the choice of action of animal which was already a function of (f2-f1). However, one cannot interpret these results as the comparison happening exclusively in SII and not in other brain areas. In Romo's work, 17% of the sampled neurons in SII had f2-f1 dependent activity. In our results, 22% of sampled neurons in SII were classified as decision-coding neurons through correlation analysis which was confirmed by fitting neuronal activity as a function of σ_2- σ_1 (the proportion of neurons with significant weight rose to about 24% during the post-stimulus delay) The proportion of neurons with choice related activity in SII in the two studies appear to be relatively consistent.

The result in line with the findings from SII in monkeys (Romo et al., 2002) indicate that although the comparison is reflected in SII, it is not yet clear whether these neurons are the ones directly participate in making the comparison and forming the choice. It is plausible that SII receives a copy of the comparison and choice that was already formed in another brain area. In order to answer this open question, further studies using techniques that can modulate the activity of neurons in SII can be designed.

The question that rises here is how and from which brain area is the information about σ_1 fed to SII at the time of comparison, for which we do not have any clear answer yet. We can speculate that information that was kept in higher brain areas can be accessible to SII at the point of comparison. The results of the work of our colleagues in the SISSA laboratory already showed that neurons in PFC (Esmaeili, 2014) and PMC (unpub. observ.) maintain the σ_1 trace in their firing rates throughout the delay and these areas can potentially provide this information to SII, although further work is required for establishing the anatomical connectivity. A comparison of major findings of the different brain areas in the task is shown schematically in Figure 4.1.

As mentioned in the results section, one of the major observations in the hippocampal population recorded was the place coding. This place coding happened after the go signal as the animal made the choice; this is simply in line with the theory of cognitive mapping (O'Keefe and Nadel, 1978) and the role of the hippocampus in navigation. We hypothesized that hippocampus has a wider participation in memory systems than the cognitive map theory gives credit for. We could not find any reasonable trace of σ_1 memory as a sustained activity during the delay in the hippocampus. However, we had another unexpected observation in the hippocampus; the choice related activity in a small subset of neurons was identified. This decision-correlated activity occurred during the post-stimulus delay and prior to animal's choice. The decision-related activity in the hippocampus ensembles had already been reported in rats doing spatial decision task in multiple-T maze (Johnson and Redish, 2007; van der Meer et al., 2010). The future path that the animal is going to take was transiently reflected in hippocampal ensembles as "lookahead". The "lookahead" activity was happening at the final choice point of the maze were the outcome can vary depending on animal choice. The authors interpreted this finding as an evidence for the engagement of hippocampus in "model-based" system of decision making

where expectations of the action outcome are the basis of the decision made. The decision neurons that are identified here are distinct in comparison with the decision-related activity that was already shown in hippocampus as it does not rely on ensemble activity, each decision neuron alone showed faithful correlation with the future choice of animal in the correct trials. We observed that the choice-correlated activity was not present in the error trials, nonetheless the power of our analysis for error trials was low as there were fewer error trials in comparison with correct trials. We identified few neurons that encoded animal action. There were confounding factors in our study of hippocampus, in the case of Ve15 from which we recorded the majority of neurons. In this case the array of electrodes was moveable in depth which made a constraint in the knowledge about the precise location of the electrode tip. We cannot be sure about the location of these decision neurons within the hippocampus. In future studies, the knowledge about the precise location of the tip of the electrode can permit further exploration of the hippocampus region. This progress will potentially enable us to identify more neurons with choice-related activity.

"A key insight from decision-making studies across different domains is that decisions can arise from multiple, parallel systems in the brain" (van der Meer et al., 2010; O'Keef and Nadel, 1978; Poldrack and Packard, 2003; Daw et al., 2005; Redish et al, 2008); So it may not be unreasonable to argue that the decision reflected in hippocampus, as observed in this study, was a copy of the decision that was already made in another area. To further investigate this possibility (hypothesis) one needs to compare the latency of the arrival of decision in hippocampal neurons with decision neurons in areas like premotor cortex. Therefore simultaneous recording from hippocampus and premotor cortex has the potential to shed light on the nature of the decision observed in hippocampal neurons and broader possibilities as suggested by van der Meer et al. (2010).

Further studies can be designed to disentangle whether or not this decision is correlated with task stimuli by introducing control trials. In possible control trial, the animal can be cued at the beginning of the trial to turn to the right or left reward spout without the necessity of attending the stimuli. If the same decision neurons show similar activity in control trials to the trials with WM stimuli presented, then it is reasonable to assume that this activity is not part of the working memory task and is more like "lookahead" behavior. Another confounding factor associated with this

study was that the number of correct trials was significantly larger than error trials. To mitigate and remove this confounding factor in a future study, one should balance the number of actual trials versus the control (sham) trials.

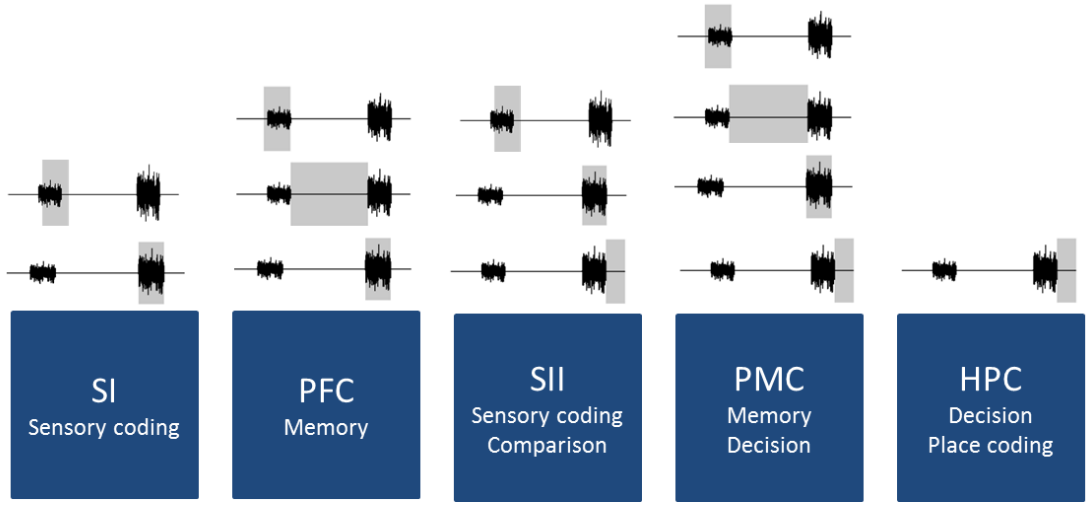

Figure 4.1. Task involvement of studied brain areas during tactile WM task. The grey shades indicate time intervals in which the neurons in a region carry significant task-related signals. SI showed σ coding during stimulus presentation and early during the delay. Prefrontal cortex showed sensory coding and trace of stimulus during delay. SII had activity relevant to comparison rule, in addition to similar sensory coding and early delay activity of SI. Premotor cortex manifested activity during the entire task timeline, including sensory coding, memory during delay and decision during the post-stimulus delay. Hippocampus showed decision-correlated activity during post-stimulus delay and place coding during the action phase. (SI, primary somatosensory cortex; PFC, prefrontal cortex; SII, secondary somatosensory cortex, PMC, premotor cortex; HPC, hippocampus)

Another finding in the hippocampal neurons was the ramping activity, which did not show any stimulus dependence. This ramping activity could be an indication of temporal dependence of the spiking activity of these neurons. Unlike the ramping neurons found in PFC of monkeys performing delayed-comparison task (Hernandez et al., 2002), there was not significant stimulus coding in our identified ramping neurons. However the precise coding of the start and end of trial through firing rate of these neurons, warrants further exploration of hippocampus for coding task timeline. The changes in the delay length in blocks of trials, can be fruitful to unravel the role of these neurons in the WM task.

In the hippocampal population, in contrast to SII sensory coding of vibratory stimulus, there was not significant evidence of sensory activity during stimulus presentation.

There are issues that still need to be considered with further analysis; for instance, differences in stimulus coding and its consequence in animal's choice, between correct and incorrect trials, is not addressed in this text. Furthermore, it is also of interest to investigate any trace of stimulus or its memory in neuronal oscillations during the delay. Zuo and colleagues, recorded simultaneously from SI and SII in rats as the animals performed a texture discrimination task using whiskers and showed that both rate and timing in these two areas govern perception (Zuo et al., 2015). However, particular characteristic of tactile WM task including the suppression of active whisking and well-defined epochs of the task which allows following the flow of information as the trial timeline evolves, suggest that further simultaneous recording from SI and SII areas can shed light on the hierarchical processing of sensory information in the context of working memory.

References

Alloway, K. D. and H. Burton (1985). "Submodality and columnar organization of the second somatic sensory area in cats." Exp Brain Res 61(1): 128-140.

Alloway, T. P. and R. G. Alloway (2010). "Investigating the predictive roles of working memory and IQ in academic attainment." J Exp Child Psychol 106(1): 20-29.

Axmacher, N., S. Lenz, S. Haupt, C. E. Elger and J. Fell (2010). "Electrophysiological signature of working and long-term memory interaction in the human hippocampus." Eur J Neurosci 31(1): 177-188.

Baddeley, A. (1992). Working memory. Science, 255(5044), 556-559.

Bedwell, S. A., E. E. Billett, J. J. Crofts and C. J. Tinsley (2014). "The topology of connections between rat prefrontal, motor and sensory cortices." Front Syst Neurosci 8.

Ben-Yakov, A. and Y. Dudai (2011). "Constructing realistic engrams: poststimulus activity of hippocampus and dorsal striatum predicts subsequent episodic memory." J Neurosci 31(24): 9032-9042.

Benison, A. M., D. M. Rector and D. S. Barth (2007). "Hemispheric mapping of secondary somatosensory cortex in the rat." J Neurophysiol 97(1): 200-207.

Bokil, H., P. Andrews, J. E. Kulkarni, S. Mehta and P. P. Mitra (2010). "Chronux: a platform for analyzing neural signals." J Neurosci Methods 192(1): 146-151.

Boyden, E. S., F. Zhang, E. Bamberg, G. Nagel and K. Deisseroth (2005). "Millisecond-timescale, genetically targeted optical control of neural activity." Nat Neurosci 8(9): 1263-1268.

Bunsey, M. and H. Eichenbaum (1996). "Conservation of hippocampal memory function in rats and humans." Nature 379(6562): 255-257.

Burgess, N., E. A. Maguire and J. O'Keefe (2002). "The human hippocampus and spatial and episodic memory." Neuron 35(4): 625-641.

Buzsaki, G. (2004). "Large-scale recording of neuronal ensembles." Nat Neurosci 7(5): 446-451.

Cannestra, A. F., N. Pouratian, S. Y. Bookheimer, N. A. Martin, D. P. Beckerand and A. W. Toga (2001). "Temporal spatial differences observed by functional MRI and human intraoperative optical imaging." Cereb Cortex 11(8): 773-782.

Carruthers, P. (2013). "Evolution of working memory." Proceedings of the National Academy of Sciences of the United States of America 110(Suppl 2): 10371-10378.

Catania, K. C. and J. H. Kaas (2001). "Areal and callosal connections in the somatosensory cortex of the star-nosed mole." Somatosens Mot Res 18(4): 303-311.

Chen, J. L., S. Carta, J. Soldado-Magraner, B. L. Schneider and F. Helmchen (2013). "Behaviour-dependent recruitment of long-range projection neurons in somatosensory cortex." Nature 499(7458): 336-340.

Cooper R, Binnie CD, Osselton JW, Prior PF, Wisman T. EEG, paediatric neurophysiology, special techniques and applications. In: Clinical Neurophysiology, Vol. 2, edited by Cooper R, Mauguiere F, Osselton JW, Prior PF, and Tedman BM. Amsterdam: Elsevier, 2003, p. 8–103.

Cowan, N. (2008). "What are the differences between long-term, short-term, and working memory?" Prog Brain Res 169: 323-338.

Daw, N.D., Niv, Y., and Dayan, P. (2005). Uncertainty-based competition between prefrontal and dorsolateral striatal systems for behavioral control. Nat. Neurosci. 8, 1704–1711.

Diamond, M. E. and E. Arabzadeh (2013). "Whisker sensory system - from receptor to decision." Prog Neurobiol 103: 28-40.

Diamond, M. E., M. von Heimendahl, P. M. Knutsen, D. Kleinfeld and E. Ahissar (2008). "'Where' and 'what' in the whisker sensorimotor system." Nat Rev Neurosci 9(8): 601-612.

Diekamp, B., T. Kalt and O. Gunturkun (2002). "Working memory neurons in pigeons." J Neurosci 22(4): Rc210.

Disbrow, E., E. Litinas, G. H. Recanzone, J. Padberg and L. Krubitzer (2003). "Cortical connections of the second somatosensory area and the parietal ventral area in macaque monkeys." J Comp Neurol 462(4): 382-399.

Dudchenko, P. A. (2004). An overview of the tasks used to test working memory in rodents. Neurosci Biobehav Rev, 28(7), 699-709. doi:10.1016/j.neubiorev.2004.09.002

Eichenbaum, H. (2000). "Hippocampus: mapping or memory?" Curr Biol 10(21): R785-787.

Eichenbaum, H. (2004). "Hippocampus: cognitive processes and neural representations that underlie declarative memory." Neuron 44(1): 109-120.

Ennaceur, A., & Delacour, J. (1988). A new one-trial test for neurobiological studies of memory in rats. 1: Behavioral data. Behav Brain Res, 31(1), 47-59.

Eslinger, P. J. and A. R. Damasio (1985). "Severe disturbance of higher cognition after bilateral frontal lobe ablation: patient EVR." Neurology 35(12): 1731-1741.

Esmaeili, V. (2014). Neuronal correlates of tactile working memory in rat barrel cortex and prefrontal cortex (Doctoral Dissertation), SISSA.

Evarts, E. V. (1968). A technique for recording activity of subcortical neurons in moving animals. Electroencephalogr Clin Neurophysiol, 24(1), 83-86.

Fassihi, A. (2012). Perception of tactile vibrations and a putative neuronal code (Doctoral Dissertation), SISSA.

Fassihi, A., A. Akrami, V. Esmaeili and M. E. Diamond (2014). "Tactile perception and working memory in rats and humans." Proc Natl Acad Sci U S A 111(6): 2331-2336.

Fuentemilla, L., W. D. Penny, N. Cashdollar, N. Bunzeck and E. Duzel (2010). "Theta-coupled periodic replay in working memory." Curr Biol 20(7): 606-612.

Fukuda, K. and E. K. Vogel (2009). "Human variation in overriding attentional capture." J Neurosci 29(27): 8726-8733.

Funahashi, S., Bruce, C. J., & Goldman-Rakic, P. S. (1989). Mnemonic coding of visual space in the monkey's dorsolateral prefrontal cortex. J Neurophysiol, 61(2), 331-349.

Fuster, J. M., & Alexander, G. E. (1971). Neuron activity related to short-term memory. Science, 173(3997), 652-654.

Hernandez, A., E. Salinas, R. Garcia and R. Romo (1997). "Discrimination in the sense of flutter: new psychophysical measurements in monkeys." J Neurosci 17(16): 6391-6400.

Hernandez, A., A. Zainos and R. Romo (2002). "Temporal evolution of a decision-making process in medial premotor cortex." Neuron 33(6): 959-972.

Hernández, A., A. Zainos and R. Romo (2000). "Neuronal correlates of sensory discrimination in the somatosensory cortex." Proceedings of the National Academy of Sciences of the United States of America 97(11): 6191-6196.

Hill, D. N., S. B. Mehta and D. Kleinfeld (2011). "Quality metrics to accompany spike sorting of extracellular signals." J Neurosci 31(24): 8699-8705.

Hollingworth, H. L. (1910). "The Central Tendency of Judgment." The Journal of Philosophy, Psychology and Scientific Methods 7(17): 461-469.

Huntley, J. D. and R. J. Howard (2010). "Working memory in early Alzheimer's disease: a neuropsychological review." Int J Geriatr Psychiatry 25(2): 121-132.

Jacobsen, C. F. (1936). Studies of cerebral function in primates. I. The functions of the frontal association areas in monkeys. Comparative Psychology Monographs, 13, 3, 1-60.

Johnson, A., and Redish, A.D. (2007). Neural ensembles in CA3 transiently encode paths forward of the animal at a decision point. J. Neurosci. 27, 12176–12189.

Kaas, A. L., H. van Mier and R. Goebel (2007). "The neural correlates of human working memory for haptically explored object orientations." Cereb Cortex 17(7): 1637-1649.

Kane, M. J. and R. W. Engle (2002). "The role of prefrontal cortex in working-memory capacity, executive attention, and general fluid intelligence: an individual-differences perspective." Psychon Bull Rev 9(4): 637-671.

Koch, C. and R. C. Reid (2012). "Neuroscience: Observatories of the mind." Nature 483(7390): 397-398.

Krubitzer, L. A. and J. H. Kaas (1990). "The organization and connections of somatosensory cortex in marmosets." J Neurosci 10(3): 952-974.

Leszczynski, M. (2011). "How Does Hippocampus Contribute to Working Memory Processing?" Frontiers in Human Neuroscience 5: 168.

Ludwig, K. A., R. M. Miriani, N. B. Langhals, M. D. Joseph, D. J. Anderson and D. R. Kipke (2009). "Using a common average reference to improve cortical neuron recordings from microelectrode arrays." J Neurophysiol 101(3): 1679-1689.

Ludwig, K. A., J. D. Uram, J. Yang, D. C. Martin and D. R. Kipke (2006). "Chronic neural recordings using silicon microelectrode arrays electrochemically deposited with a poly(3,4-ethylenedioxythiophene) (PEDOT) film." J Neural Eng 3(1): 59-70.

McCabe, D. P., H. L. Roediger, M. A. McDaniel, D. A. Balota and D. Z. Hambrick (2010). "The relationship between working memory capacity and executive functioning: evidence for a common executive attention construct." Neuropsychology 24(2): 222-243.

McDowell, S., J. Whyte and M. D'Esposito (1997). "Working memory impairments in traumatic brain injury: evidence from a dual-task paradigm." Neuropsychologia 35(10): 1341-1353.

Melzer, P., G. C. Champney, M. J. Maguire and F. F. Ebner (2006). "Rate code and temporal code for frequency of whisker stimulation in rat primary and secondary somatic sensory cortex." Exp Brain Res 172(3): 370-386.

Menon, R. S. and S. G. Kim (1999). "Spatial and temporal limits in cognitive neuroimaging with fMRI." Trends Cogn Sci 3(6): 207-216.

Milner, B. (1982). "Some cognitive effects of frontal-lobe lesions in man." Philos Trans R Soc Lond B Biol Sci 298(1089): 211-226.

O'Keefe, J. (1978). The hippocampus as a cognitive map / John O'Keefe and Lynn Nadel. Oxford : New York, Clarendon Press ; Oxford University Press.

O'Keefe, J. and J. Dostrovsky (1971). "The hippocampus as a spatial map. Preliminary evidence from unit activity in the freely-moving rat." Brain Res 34(1): 171-175.

Offner, F. F. (1950). "The EEG as potential mapping: the value of the average monopolar reference." Electroencephalogr Clin Neurophysiol 2(2): 213-214.

Olton, D. S., & Samuelson, R. J. (1976). Remembrance of places passed: Spatial memory in rats. Journal of Experimental Psychology: Animal Behavior Processes, 2(2), 97-116. doi:10.1037/0097-7403.2.2.97

Olton, D. S., Becker, J. T. and Handelmann, G. E. (1979). Hippocampus, space, and memory. Behavioral and Brain Sciences, 2, pp 313-322 doi:10.1017/S0140525X00062713

Osselton, J. W. (1965). "Acquisition of EEG data by bipolar, unipolar and average reference methods: a theoretical comparison." Electroencephalogr Clin Neurophysiol 19(5): 527-528.

Paxinos, G. W., S. (2007). "The rat brain in stereotaxic coordinates."

Penner, M. R. and S. J. Mizumori (2012). "Neural systems analysis of decision making during goal-directed navigation." Prog Neurobiol 96(1): 96-135.

Pesaran, B., J. S. Pezaris, M. Sahani, P. P. Mitra and R. A. Andersen (2002). "Temporal structure in neuronal activity during working memory in macaque parietal cortex." Nat Neurosci 5(8): 805-811.

Pierret, T., P. Lavallee and M. Deschenes (2000). "Parallel streams for the relay of vibrissal information through thalamic barreloids." J Neurosci 20(19): 7455-7462.

Poldrack, R.A., and Packard, M.G. (2003). Competition among multiple memory systems: converging evidence from animal and human brain studies. Neuropsychologia 41, 245–251.

Prasad, A. and J. C. Sanchez (2012). "Quantifying long-term microelectrode array functionality using chronic in vivo impedance testing." J Neural Eng 9(2): 026028.

Prescott, T. J., M. E. Diamond and A. M. Wing (2011). "Active touch sensing." Philos Trans R Soc Lond B Biol Sci 366(1581): 2989-2995.

Preuschhof, C., H. R. Heekeren, B. Taskin, T. Schubert and A. Villringer (2006). "Neural correlates of vibrotactile working memory in the human brain." J Neurosci 26(51): 13231-13239.

Quian Quiroga, R. (2009). "What is the real shape of extracellular spikes?" J Neurosci Methods 177(1): 194-198.

Quiroga, R. Q., Z. Nadasdy and Y. Ben-Shaul (2004). "Unsupervised spike detection and sorting with wavelets and superparamagnetic clustering." Neural Comput 16(8): 1661-1687.

Ranganath, C. and M. D'Esposito (2001). "Medial temporal lobe activity associated with active maintenance of novel information." Neuron 31(5): 865-873.

Redish, A.D., Jensen, S., and Johnson, A. (2008). A unified framework for addiction: vulnerabilities in the decision process. Behav. Brain Sci. 31, 415–437.

Reep, R. L., G. S. Goodwin and J. V. Corwin (1990). "Topographic organization in the corticocortical connections of medial agranular cortex in rats." J Comp Neurol 294(2): 262-280.

Romo, R., C. D. Brody, A. Hernandez and L. Lemus (1999). "Neuronal correlates of parametric working memory in the prefrontal cortex." Nature 399(6735): 470-473.

Romo, R., A. Hernandez, A. Zainos, L. Lemus and C. D. Brody (2002). "Neuronal correlates of decision-making in secondary somatosensory cortex." Nat Neurosci 5(11): 1217-1225.

Romo, R. and E. Salinas (2003). "Flutter discrimination: neural codes, perception, memory and decision making." Nat Rev Neurosci 4(3): 203-218.

Rothblat, L. A., & Hayes, L. L. (1987). Short-term object recognition memory in the rat: nonmatching with trial-unique junk stimuli. Behav Neurosci, 101(4), 587-590.

Safaai, H., Y. Zuo, M. Maravall, S. Panzeri and M. E. Diamond (2014). "Hierarchical flow of sensory information in rat somatosensory cortex." BMC Neuroscience 15(1): 1-2.

Schwark, H. D., H. Esteky and E. G. Jones (1992). "Corticocortical connections of cat primary somatosensory cortex." Exp Brain Res 91(3): 425-434.

Scoville, W. B. and B. Milner (1957). "Loss of recent memory after bilateral hippocampal lesions." J Neurol Neurosurg Psychiatry 20(1): 11-21.

Slepian, D. and H. O. Pollack (1961). "Prolate spheroidal wavefunctions: Fourier analysis and uncertainty I." Bell System Tech Journal 40: 43-63.

Smith, J. B. and K. D. Alloway (2013). "Rat whisker motor cortex is subdivided into sensory-input and motor-output areas." Front Neural Circuits 7: 4.

Stelzer, J., G. Lohmann, K. Mueller, T. Buschmann and R. Turner (2014). "Deficient approaches to human neuroimaging." Frontiers in Human Neuroscience 8: 462.

van der Meer, M. A. A., A. Johnson, N. C. Schmitzer-Torbert and A. D. Redish (2010). "Triple Dissociation of Information Processing in Dorsal Striatum, Ventral Striatum, and Hippocampus on a Learned Spatial Decision Task." Neuron 67(1): 25-32.

Veit, L., Hartmann, K., & Nieder, A. (2014). Neuronal correlates of visual working memory in the corvid endbrain. J Neurosci, 34(23), 7778-7786. doi:10.1523/jneurosci.0612-14.2014

Weber, E. H. (1996). E.H. Weber on the tactile senses. E. H. Weber, E. H. Weber, H. E. Ross and D. J. Murray. Hove :, Erlbaum (UK) Taylor & Francis.

Wood, E. R., P. A. Dudchenko and H. Eichenbaum (1999). "The global record of memory in hippocampal neuronal activity." Nature 397(6720): 613-616.

Wood, E. R., Dudchenko, P. A., Robitsek, R. J., & Eichenbaum, H. (2000). Hippocampal neurons encode information about different types of memory episodes occurring in the same location. Neuron, 27(3), 623-633.

Yang, H., S. E. Kwon, K. S. Severson and D. H. O'Connor (2016). "Origins of choice-related activity in mouse somatosensory cortex." Nat Neurosci 19(1): 127-134.

Zakiewicz, I. M., J. G. Bjaalie and T. B. Leergaard (2014). "Brain-wide map of efferent projections from rat barrel cortex." Front Neuroinform 8.

Zuo, Y., H. Safaai, G. Notaro, A. Mazzoni, S. Panzeri and M. E. Diamond (2015). "Complementary contributions of spike timing and spike rate to perceptual decisions in rat S1 and S2 cortex." Curr Biol 25(3): 357-363.

Appendix

Working memory performance of individual rats before the surgery is shown in Figure A.1, Figure A.2 and Figure A.3.

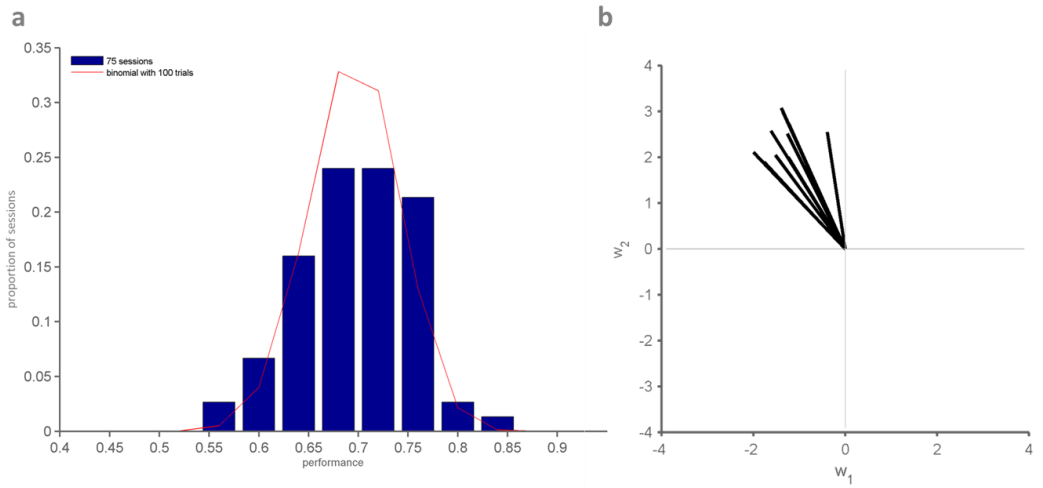

Figure A.1. Behavior of sht2 before surgery and implant in SII, (a) The performance of the rat across sessions followed a binomial distribution. (b) Weights of σ1 and σ2 in animal choice are represented by w1 and w2.

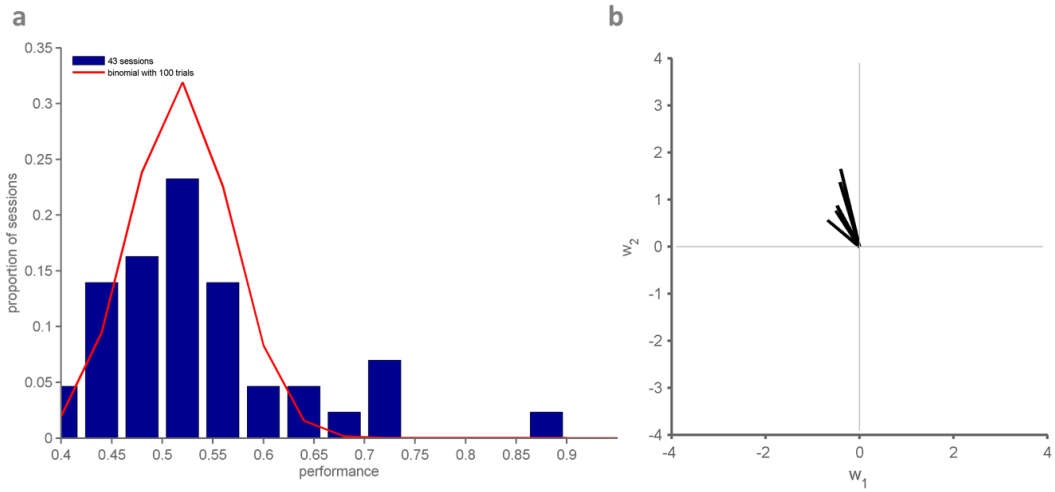

Figure A.2. Behavior of ar22 before surgery and implant in hippocampus. Panels are similar to Figure A.1.

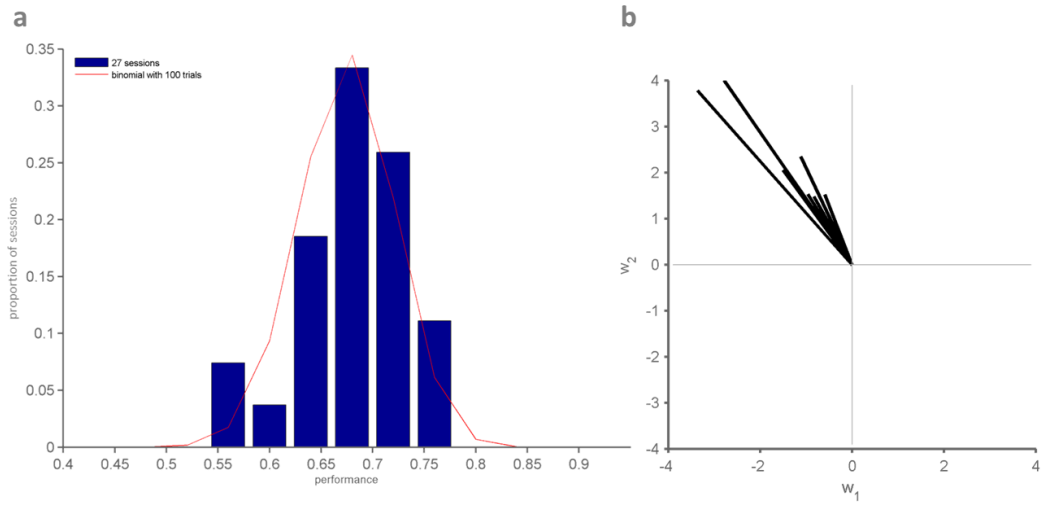

Figure A.3. Behavior of ar26 before surgery and implant in hippocampus. Panels are similar to Figure A.1.